

# Updated Global Fits of the SM and MSSM to Electroweak Precision Data

W. de Boer<sup>i1</sup>, A. Dabelstein<sup>iii2</sup>, W. Hollik<sup>ii3</sup>,  
W. Mösle<sup>ii4</sup>, U. Schwickerath<sup>i5</sup>,

- i) Inst. für Experimentelle Kernphysik, Univ. Karlsruhe,  
Postfach 6980, D-76128 Karlsruhe, Germany*  
*ii) Inst. für Theoretische Physik, Univ. Karlsruhe,  
Postfach 6980, D-76128 Karlsruhe, Germany*  
*iii) Inst. für Theoretische Physik, Univ. München,  
James Franck Straße, D-85747 Garching, Germany*

## Abstract

The Minimal supersymmetric extension of the Standard Model (MSSM) with light stops, charginos or pseudoscalar Higgs bosons has been suggested as an explanation of the too high value of the branching ratio of the  $Z^0$  boson into  $b$  quarks ( $R_b$  anomaly). A program including all radiative corrections to the MSSM at the same level as the radiative corrections to the SM has been developed and used to perform global fits to all electroweak data from LEP, SLC and the Tevatron. Recent updates on electroweak data, which have been presented at the Warsaw Conference in summer 1996, reduce the  $R_b$  anomaly from a  $3.2\sigma$  to a  $1.8\sigma$  effect, which improves the probability in the SM from 8% to 24%. Although the MSSM can fully explain the remaining deviation of  $R_b$  from the SM value, its probability is not better because of the larger number of free parameters. The best fitted values of the strong coupling constant at the  $M_Z$  scale in the  $\overline{MS}$  renormalization scheme is  $0.120 \pm 0.003$  for the SM and  $0.116 \pm 0.005$  ( $0.119 \pm 0.005$ ) for the MSSM with low (high) values of  $\tan\beta$ . The derived quantity  $\sin^2\theta_{\overline{MS}}$  equals  $0.2317 \pm 0.0004$  ( $0.2315 \pm 0.0004$ ) for the SM (MSSM).

---

<sup>1</sup>Email: wim.de.boer@cern.ch

<sup>2</sup>E-mail: Andreas.Dabelstein@tu-muenchen.de

<sup>3</sup>E-mail: hollik@itpaxp3.physik.uni-karlsruhe.de

<sup>4</sup>E-mail: wm@itpaxp1.physik.uni-karlsruhe.de

<sup>5</sup>E-mail: Ulrich.Schwickerath@cern.ch

# 1 Introduction

Old LEP data showed a too high value of  $R_b$  ( $3.2\sigma$ ) and a too low value of  $R_c$  ( $2\sigma$ ) where  $R_{b(c)}$  is the ratio  $R_{b(c)} = \Gamma_{Z^0 \rightarrow b\bar{b}(c\bar{c})} / \Gamma_{Z^0 \rightarrow q\bar{q}}$ . In the past it has been shown by several groups that it is possible to increase  $R_b$  using minimal supersymmetric models (MSSM) with light charginos, stops or Higgses, which yield positive contributions to the  $Zb\bar{b}$  vertex, although no improvement in  $R_c$  could be obtained[1]-[9]. Recent updates of electroweak data, which have been presented at the Warsaw Conference[10] show no deviation of  $R_c$  anymore and a value of  $R_b$  which is  $1.8\sigma$  above the SM value. Such a moderate deviation in  $R_b$  can be either due to a fluctuation in statistical or systematic errors or may originate from genuine MSSM contributions.

In this paper we perform an equivalent analysis of all electroweak data both in the SM and its supersymmetric extension, using all actual electroweak data from Tevatron [11, 12], LEP and SLC [13, 10], the measurement of  $\frac{BR(b \rightarrow s\gamma)}{BR(b \rightarrow ce\bar{\nu})}$  from CLEO [14] and limits on the masses of supersymmetric particles [1, 15, 16, 17, 18, 19]. For the SM predictions the ZFITTER program[20] was used, while for the MSSM predictions the SUSYFITTER program[21], which will be discussed below, was used. In both cases MINUIT[22] was used as  $\chi^2$  minimizer in order to obtain the optimum parameter values.

## 2 $Z^0$ boson on-resonance observables

At the  $Z$  boson resonance two classes of precision observables are available:

a) inclusive quantities:

- the partial leptonic and hadronic decay width  $\Gamma_{f\bar{f}}$ ,
- the total decay width  $\Gamma_Z$ ,
- the hadronic peak cross section  $\sigma_h$ ,
- the ratio of the hadronic to the electronic decay width of the  $Z$  boson:  $R_h$ ,
- the ratio of the partial decay width for  $Z \rightarrow c\bar{c}(b\bar{b})$  to the hadronic width,  $R_c, R_b$ .

b) asymmetries and the corresponding mixing angles:

- the *forward-backward* asymmetries  $A_{FB}^f$ ,
- the *left-right* asymmetries  $A_{LR}^f$ ,
- the  $\tau$  polarization  $P_\tau$ ,
- the effective weak mixing angles  $\sin^2 \theta_{eff}^f$ .

Together with the quantity  $\Delta r$  in the correlation of the  $W$  mass to the electroweak input parameters  $G_\mu$ ,  $M_Z$  and  $\alpha_{em}$ , this set of precision observables is convenient for a numerical analysis of the supersymmetric parameter space. In the following the observables defined above are expressed with the help of effective couplings.

## 2.1 The effective $Z$ - $f$ - $f$ couplings

The coupling of the  $Z$  boson to fermions  $f$  can be expressed by effective vector and axial vector coupling constants  $v_{eff}^f, a_{eff}^f$  in terms of the NC vertex:

$$J_{NC}^\mu = \frac{e}{2s_W c_W} \gamma^\mu (v_{eff}^f - a_{eff}^f \gamma_5), \quad (1)$$

where the convention is introduced :  $c_W^2 = \cos^2 \theta_W = 1 - s_W^2 = M_W^2/M_Z^2$  [23]. Input parameters are the  $\mu$  decay constant  $G_\mu = 1.166392 \times 10^{-5} \text{ GeV}^{-2}$ ,  $\alpha_{EM} = 1/137.036$  and the mass of the  $Z^0$  boson  $M_Z = 91.1884 \text{ GeV}$ . The mass of the  $W$  boson is related to these input parameters through:

$$\frac{G_\mu}{\sqrt{2}} = \frac{\pi \alpha_{EM}}{2s_W^2 M_W^2} \cdot \frac{1}{1 - \Delta r_{MSSM}(\alpha_{EM}, M_W, M_Z, m_t, \dots)}, \quad (2)$$

where the complete MSSM one-loop contributions are parameterized by the quantity  $\Delta r_{MSSM}$ [24]. Leading higher order Standard Model corrections[25, 26] to the quantity  $\Delta r$  are included in the calculation.

The effective couplings  $v_{eff}^f, a_{eff}^f$  can be written as:

$$\begin{aligned} v_{eff}^f &= \sqrt{Z_Z} (v^f + \Delta v^f + Z_M Q_f) \\ a_{eff}^f &= \sqrt{Z_Z} (a^f + \Delta a^f). \end{aligned} \quad (3)$$

$v^f$  and  $a^f$  are the tree-level vector and axial vector couplings:

$$v^f = I_3^f - 2Q_f s_W^2, \quad a^f = I_3^f. \quad (4)$$

$Z_Z, Z_M$  are given in eq. (10). The complete MSSM one-loop contributions of the non-universal finite vector and axial vector couplings  $\Delta v^f, \Delta a^f$  have been calculated[21], together with the leading two-loop Standard Model contributions[25, 26, 27]. They are derived in the 't Hooft-Feynman gauge and in the on-shell renormalization scheme[28]. Fig. 1 shows the MSSM one-loop  $Z \rightarrow f\bar{f}$  vertex correction diagrams.

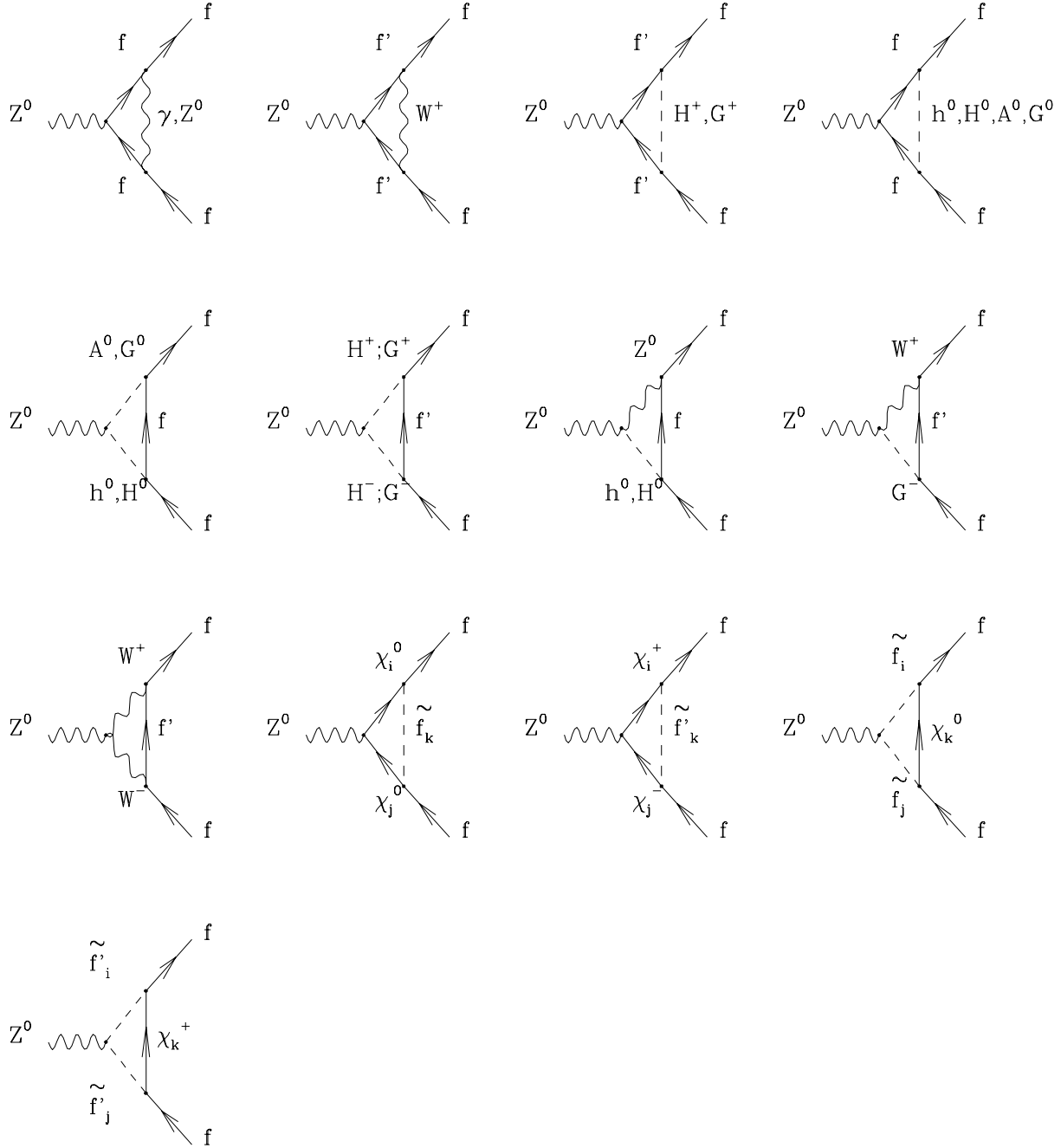


Figure 1: MSSM one-loop  $Z \rightarrow f\bar{f}$  vertex correction diagrams.  $i, j, k = 1, \dots, 2(4)$  are chargino, neutralino and sfermions indices. No particle permutations are shown.

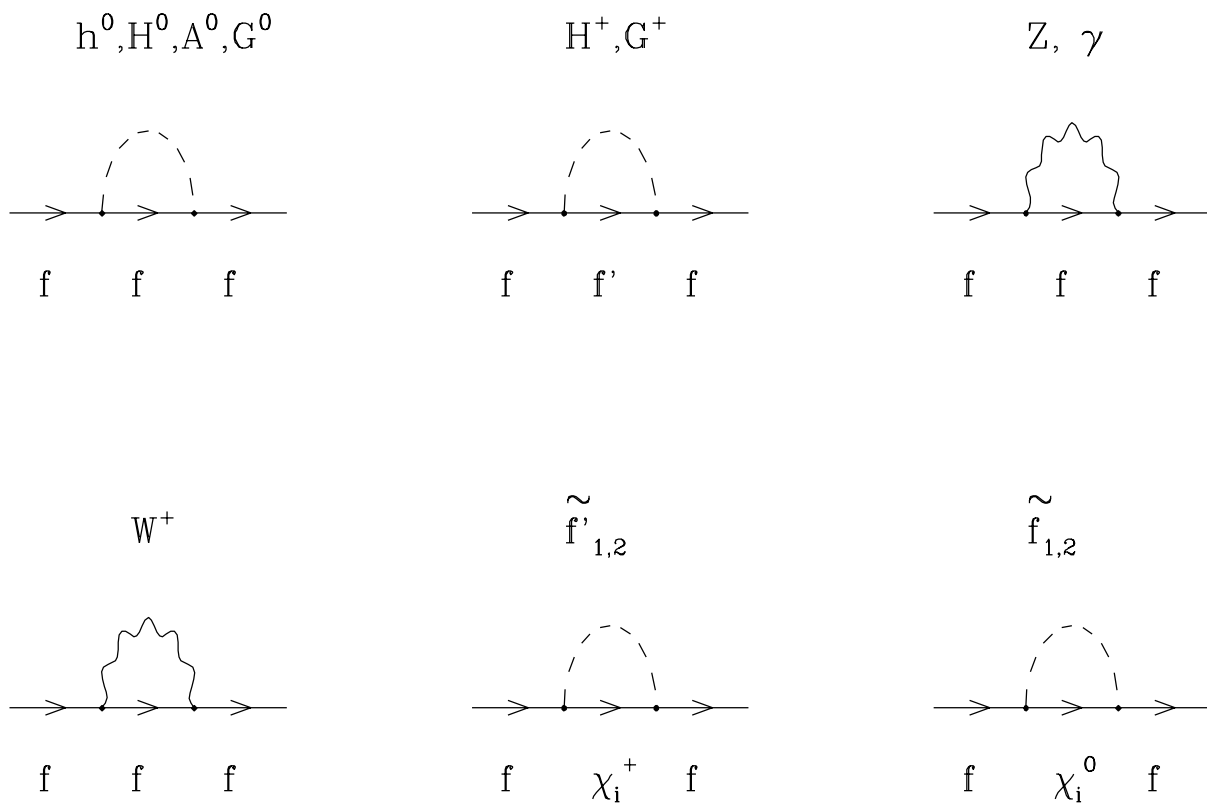


Figure 2: MSSM fermion self-energies.

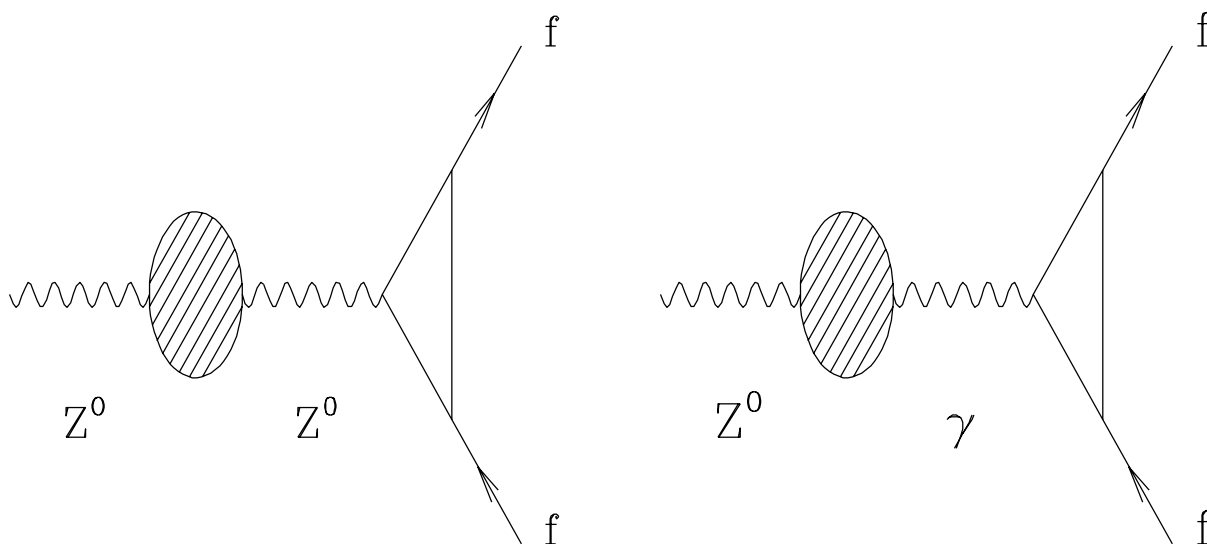


Figure 3:  $Z$  boson wave function renormalization.

The non-universal contributions can be written in the following way:

$$\begin{aligned}\Delta v_f &= F_V^{SM} + \Delta F_V, \\ \Delta a_f &= F_A^{SM} + \Delta F_A.\end{aligned}$$

The Standard Model form factors  $F_{V,A}^{SM}$  corresponding to the diagrams of figs. 1 and 2 can be found e.g in refs. [28, 25]. The diagrams with a virtual photon are listed for completeness in the figures. They are not part of the effective weak couplings but are treated separately in the QED corrections, together with real photon bremsstrahlung. The non-standard contributions are summarized by

$$\begin{aligned}\Delta F_V &= \sum_i F_V^{(i)} + v_f \delta Z_V^f + a_f \delta Z_A^f \\ \Delta F_A &= \sum_i F_A^{(i)} + v_f \delta Z_A^f + a_f \delta Z_V^f\end{aligned}$$

where the sum extends over the diagrams of fig. 1 with internal charged and neutral Higgs bosons, charginos, neutralinos and scalar fermions, each diagram contributing

$$F_V^{(i)} \gamma_\mu - F_A^{(i)} \gamma_\mu \gamma_5$$

to the  $Zff$ -vertex. The self-energy diagrams of fig. 2 with internal neutral Higgs, chargino, neutralino and sfermion lines determine the field renormalization constants

$$\begin{aligned}\delta Z_V^f &= -\Sigma_V(m_f^2) - 2m_f^2[\Sigma'_V(m_f^2) + \Sigma'_S(m_f^2)] \\ \delta Z_A^f &= \Sigma_A(m_f^2)\end{aligned}\tag{5}$$

with the scalar functions  $\Sigma_{V,A,S}$  in the decomposition of the fermion self-energy according to

$$\Sigma = \not{p}\Sigma_V + \not{p}\gamma_5\Sigma_A + m_f\Sigma_S.$$

The contributions from the Higgs sector are given explicitly in ref. [29]. For the genuine SUSY diagrams, the couplings for charginos, neutralinos and sfermions are taken from [31], together with the diagonalization matrices given in section 3.

The universal propagator corrections from the finite  $Z$  boson wave function renormalization  $Z_Z$  and the  $\gamma Z$  mixing  $Z_M$  are derived from the  $(\gamma, Z)$  propagator matrix. The inverse matrix is:

$$(\Delta_{\mu\nu})^{-1} = ig_{\mu\nu} \begin{pmatrix} k^2 + \hat{\Sigma}_\gamma(k^2) & \hat{\Sigma}_{\gamma Z}(k^2) \\ \hat{\Sigma}_{\gamma Z}(k^2) & k^2 - M_Z^2 + \hat{\Sigma}_Z(k^2) \end{pmatrix},\tag{6}$$

where  $\hat{\Sigma}_\gamma$ ,  $\hat{\Sigma}_Z$ ,  $\hat{\Sigma}_{\gamma Z}$  are the renormalized self energies and mixing. They are obtained by summing the loop diagrams, shown symbolically in fig.3, and the counter terms and can be found in ref. [30].

The entries in the  $(\gamma, Z)$  propagator matrix:

$$\Delta_{\mu\nu} = -ig_{\mu\nu} \begin{pmatrix} \Delta_\gamma & \Delta_{\gamma Z} \\ \Delta_{\gamma Z} & \Delta_Z \end{pmatrix},\tag{7}$$

are given by:

$$\begin{aligned}
\Delta_\gamma(k^2) &= \frac{1}{k^2 + \hat{\Sigma}_\gamma(k^2) - \frac{\hat{\Sigma}_{\gamma Z}^2(k^2)}{k^2 - M_Z^2 + \hat{\Sigma}_Z(k^2)}} \\
\Delta_Z(k^2) &= \frac{1}{k^2 - M_Z^2 + \hat{\Sigma}_Z(k^2) - \frac{\hat{\Sigma}_{\gamma Z}^2(k^2)}{k^2 + \hat{\Sigma}_\gamma(k^2)}} \\
\Delta_{\gamma Z}(k^2) &= -\frac{\hat{\Sigma}_{\gamma Z}(k^2)}{[k^2 + \hat{\Sigma}_\gamma(k^2)][k^2 - M_Z^2 + \hat{\Sigma}_Z(k^2)] - \hat{\Sigma}_{\gamma Z}^2(k^2)}. \tag{8}
\end{aligned}$$

The renormalization condition to define the mass of the  $Z$  boson is given by the pole of the propagator matrix (eq. 6). The pole  $k^2 = M_Z^2$  is the solution of the equation:

$$\text{Re}[(M_Z^2 + \hat{\Sigma}_\gamma(M_Z^2))\hat{\Sigma}_Z(k^2) - \hat{\Sigma}_{\gamma Z}^2(M_Z^2)] = 0. \tag{9}$$

Eq. (8) yields the wave function renormalization  $Z_Z$  and mixing  $Z_M$ :

$$\begin{aligned}
Z_Z &= \text{Res}_{M_Z} \Delta_Z = \frac{1}{1 + \text{Re} \hat{\Sigma}'_Z(k^2) - \text{Re} \left( \frac{\hat{\Sigma}_{\gamma Z}^2(k^2)}{k^2 + \hat{\Sigma}_\gamma(k^2)} \right)'} \Bigg|_{k^2=M_Z^2} \\
Z_M &= -\frac{\hat{\Sigma}_{\gamma Z}(M_Z^2)}{M_Z^2 + \hat{\Sigma}_\gamma(M_Z^2)}. \tag{10}
\end{aligned}$$

## 2.2 $Z$ boson observables

The fermionic  $Z$  boson partial decay widths  $\Gamma_{f\bar{f}}$  can be written as follows:

1)  $f \neq b$ :

$$\begin{aligned}
\Gamma_{f\bar{f}} &= \frac{N_C \sqrt{2} G_\mu M_Z^3}{12\pi} (1 - \Delta r_{MSSM}) \left[ (v_{eff}^f)^2 + (a_{eff}^f)^2 \left(1 - \frac{6m_f^2}{M_Z^2}\right) \right] \\
&\cdot \left(1 + \frac{3\alpha_{EM}}{4\pi} Q_f^2\right) (1 + \delta_{QCD}^f), \tag{11}
\end{aligned}$$

where

$$\delta_{QCD}^f = \begin{cases} 0 & , f = \text{leptons} \\ \frac{\alpha_s}{\pi} + 1.405 \left(\frac{\alpha_s}{\pi}\right)^2 - 12.8 \left(\frac{\alpha_s}{\pi}\right)^3 - \frac{Q_f^2 \alpha_{\alpha_s}}{4\pi^2} & , f = \text{quarks} \end{cases}. \tag{12}$$

2)  $f = b$ :

$$\begin{aligned}
\Gamma_{b\bar{b}} &= \frac{N_C \sqrt{2} G_\mu M_Z^3}{12\pi} (1 - \Delta r_{MSSM}) \left[ (v_{eff}^b)^2 + (a_{eff}^b)^2 \right] \\
&\cdot \left(1 + \frac{3\alpha_{EM}}{4\pi} Q_b^2\right) (1 + \delta_{QCD}^b) + \Delta\Gamma_{b\bar{b}}. \tag{13}
\end{aligned}$$

In  $\Delta\Gamma_{b\bar{b}}$  the  $b$  quark specific finite mass terms with QCD corrections [27] are included.  $\delta_{QCD}^b$  is given in eq. (12).

The total decay width  $\Gamma_Z$  is the sum of the contributions from leptons and quarks:

$$\Gamma_Z = \sum_f \Gamma_{f\bar{f}} . \quad (14)$$

In the following  $\Gamma_{had} = \sum_q \Gamma_{q\bar{q}}$  is the hadronic decay width of the  $Z$  boson.

The hadronic peak cross section is defined as

$$\sigma_h = \frac{12\pi}{M_Z^2} \frac{\Gamma_{ee}\Gamma_{had}}{\Gamma_Z^2} . \quad (15)$$

The ratio of the hadronic to the electronic decay width is defined as

$$R_e = \frac{\Gamma_{had}}{\Gamma_{ee}} . \quad (16)$$

The ratio of the partial decay width for  $Z \rightarrow b\bar{b} (c\bar{c})$  to the total hadronic decay width is given by

$$R_{b(c)} = \frac{\Gamma_{b\bar{b}(c\bar{c})}}{\Gamma_{had}} . \quad (17)$$

The following quantities and observables depend on the ratio of the vector to axial vector coupling. The effective flavour dependent weak mixing angle can be written as

$$\sin^2 \theta_{eff}^f = \frac{1}{4|Q_f|} \left( 1 - \frac{v_{eff}^f}{a_{eff}^f} \right) . \quad (18)$$

The *left-right* asymmetries are given by

$$A_{LR}^f = \mathcal{A}^f = \frac{2 v_{eff}^f / a_{eff}^f}{1 + (v_{eff}^f / a_{eff}^f)^2} , \quad (19)$$

while the *forward-backward* asymmetries can be written as

$$A_{FB}^f = \frac{3}{4} \mathcal{A}^e \mathcal{A}^f . \quad (20)$$

## 3 The MSSM

### 3.1 Higgs sector

The scalar sector of the MSSM is completely determined by the value of  $\tan\beta = v_2/v_1$  and the pseudoscalar mass  $M_A$ , together with the radiative corrections. The latter ones are taken into account in terms of the effective potential approximation with the leading terms  $\sim m_t^4$ , including the mixing in the scalar top system [32]. In this way, the coupling constants of the various Higgs particles to gauge bosons and fermions can be taken over from [31] substituting only the scalar mixing angle  $\alpha$  by the improved effective mixing angle which is obtained from the diagonalization of the scalar mass matrix.

### 3.2 Sfermion sector

The physical masses of squarks and sleptons are given by the eigenvalues of the  $2 \times 2$  mass matrix:

$$\mathcal{M}_{\tilde{f}}^2 = \begin{pmatrix} M_{\tilde{Q}}^2 + m_f^2 + M_Z^2(I_3^f - Q_f s_W^2) \cos 2\beta & m_f(A_f + \mu\{\cot \beta, \tan \beta\}) \\ m_f(A_f + \mu\{\cot \beta, \tan \beta\}) & M_{\{\tilde{U}, \tilde{D}\}}^2 + m_f^2 + M_Z^2 Q_f s_W^2 \cos 2\beta \end{pmatrix}, \quad (21)$$

with SUSY soft breaking parameters  $M_{\tilde{Q}}$ ,  $M_{\tilde{U}}$ ,  $M_{\tilde{D}}$ ,  $A_f$ , and  $\mu$ . It is convenient to use the following notation for the off-diagonal entries in eq. (21):

$$A'_f = A_f + \mu\{\cot \beta, \tan \beta\}. \quad (22)$$

Scalar neutrinos appear only as left-handed mass eigenstates. Up and down type sfermions in (21) are distinguished by setting  $f=u,d$  and the  $\{u, d\}$  entries in the parenthesis. Since the non-diagonal terms are proportional to  $m_f$ , it seems natural to assume unmixed sfermions for the lepton and quark case except for the scalar top sector. The  $\tilde{t}$  mass matrix is diagonalized by a rotation matrix with a mixing angle  $\Phi_{mix}$ . Instead of  $M_{\tilde{Q}}$ ,  $M_{\tilde{U}}$ ,  $M_{\tilde{D}}$ ,  $A'_t$  for the  $\tilde{b}, \tilde{t}$  system the physical squark masses  $m_{\tilde{b}_L}, m_{\tilde{b}_R}, m_{\tilde{t}_2}$  can be used together with  $A'_t$  or, alternatively, the stop mixing angle  $\Phi_{mix}$ . For simplicity we assume  $m_{\tilde{b}_L} = m_{\tilde{b}_R}$ , and  $\tilde{u}, \tilde{d}, \tilde{c}, \tilde{s}$  to have masses equal to the  $\tilde{b}$  squark mass.

A possible mass splitting between  $\tilde{b}_L - \tilde{t}_L$  yields a contribution to the  $\rho$ -parameter  $\rho = 1 + \Delta\rho$  in terms of [24]:<sup>6</sup>

$$\Delta\rho_{\tilde{b}-\tilde{t}}^0 = \frac{3\alpha_{EM}}{16\pi s_W^2 M_W^2} \left( m_{\tilde{b}_L}^2 + m_{\tilde{t}_L}^2 - 2 \frac{m_{\tilde{b}_L}^2 m_{\tilde{t}_L}^2}{m_{\tilde{b}_L}^2 - m_{\tilde{t}_L}^2} \log \frac{m_{\tilde{b}_L}^2}{m_{\tilde{t}_L}^2} \right). \quad (23)$$

As a universal loop contribution, it enters the quantity

$$\Delta r \simeq \Delta\alpha_{EM} - \frac{c_W^2}{s_W^2} \Delta\rho + \dots \quad (24)$$

and all the  $Z$  boson widths

$$\Gamma_{f\bar{f}} \sim 1 + \Delta\rho + \dots$$

and is thus significantly constrained by the data on  $M_W$  and the leptonic widths.

### 3.3 Chargino/Neutralino sector

The chargino (neutralino) masses and the mixing angles in the gaugino couplings are calculated from soft breaking parameters  $M_1, M_2$  and  $\mu$  in the chargino (neutralino) mass matrix[31]. The validity of the GUT relation  $M_1 = 5/3 \tan^2 \theta_W M_2$  is assumed.

The chargino  $2 \times 2$  mass matrix is given by

$$\mathcal{M}_{\tilde{\chi}^\pm} = \begin{pmatrix} M_2 & M_W \sqrt{2} \sin \beta \\ M_W \sqrt{2} \cos \beta & -\mu \end{pmatrix}, \quad (25)$$

---

<sup>6</sup>The superscript  $\Delta\rho^0$  indicates that no left-right mixing is present.

with the SUSY soft breaking parameters  $\mu$  and  $M_2$  in the diagonal matrix elements. The physical chargino mass states  $\tilde{\chi}_i^\pm$  are the rotated wino and charged Higgsino states:

$$\begin{aligned}\tilde{\chi}_i^+ &= V_{ij}\psi_j^+ \\ \tilde{\chi}_i^- &= U_{ij}\psi_j^- ; i, j = 1, 2 .\end{aligned}\tag{26}$$

$V_{ij}$  and  $U_{ij}$  are unitary chargino mixing matrices obtained from the diagonalization of the mass matrix eq. 25:

$$U^* \mathcal{M}_{\tilde{\chi}^\pm} V^{-1} = \text{diag}(m_{\tilde{\chi}_1^\pm}, m_{\tilde{\chi}_2^\pm}) .\tag{27}$$

The neutralino  $4 \times 4$  mass matrix can be written as:

$$\mathcal{M}_{\tilde{\chi}^0} = \begin{pmatrix} M_1 & 0 & -M_Z \sin \theta_W \cos \beta & M_Z \sin \theta_W \sin \beta \\ 0 & M_2 & M_Z \cos \theta_W \cos \beta & -M_Z \cos \theta_W \sin \beta \\ -M_Z \sin \theta_W \cos \beta & M_Z \cos \theta_W \cos \beta & 0 & \mu \\ M_Z \sin \theta_W \sin \beta & -M_Z \cos \theta_W \sin \beta & \mu & 0 \end{pmatrix}\tag{28}$$

where the diagonalization can be obtained by the unitary matrix  $N_{ij}$ :

$$N^* \mathcal{M}_{\tilde{\chi}^0} N^{-1} = \text{diag}(m_{\tilde{\chi}_1^0}) .\tag{29}$$

The elements  $U_{ij}$ ,  $V_{ij}$ ,  $N_{ij}$  of the diagonalization matrices enter the couplings of the charginos, neutralinos and sfermions to fermions and gauge bosons, as explicitly given in ref. [31]. Note that our sign convention on the parameter  $\mu$  is opposite to that of ref. [31].

experimental limits	
$\tilde{m}_{\tilde{\chi}_{1,2}^\pm}$	> 65 GeV
$\tilde{m}_{\tilde{\chi}_1^0}$	> 13 GeV
$\tilde{m}_{\tilde{\chi}_2^0}$	> 35 GeV
$\tilde{m}_{\tilde{\chi}_{3,4}^0}$	> 60 GeV
$\Gamma_{Z \rightarrow \text{neutralinos}}$	< 2 MeV
$\tilde{m}_{\tilde{t}_{1,2}}$	> 48 GeV
$m_h, m_H, m_A, m_{H^\pm}$	> 50 GeV

Table 1: Mass limits assumed for the optimized fits.

## 4 Results

### 4.1 Chargino Masses

As mentioned before the low  $\tan \beta$  scenario of the MSSM needs a light right handed stop and light higgsino-like chargino for a larger value of  $R_b$ , whereas in the high  $\tan \beta$  scenario one needs in addition a light pseudoscalar Higgs  $A$  [1, 3]. A higgsino-like chargino can be obtained for a low value of the parameter  $\mu$  in the mass matrix (eq. 25). Figs. 4 and 5 show the dependence

Symbol	measurement	best fit observables					
		SM		MSSM			
tan $\beta$ and pull		pull		1.6	pull	34	pull
		$M_Z$ [GeV]	$91.1863 \pm 0.0020$	91.1861	0.08	91.1863	0.00
$\Gamma_Z$ [GeV]	$2.4946 \pm 0.0027$	2.4959	-0.49	2.4946	0.00	2.4939	0.24
$\sigma_h$ [nb]	$41.508 \pm 0.056$	41.466	0.75	41.4607	0.84	41.449	1.06
$R_l$	$20.778 \pm 0.029$	20.756	0.74	20.7690	0.31	20.772	0.21
$A_{FB}^l$	$0.0174 \pm 0.0010$	0.0159	1.48	0.0162	1.22	0.0161	1.25
$R_b$	$0.2178 \pm 0.0011$	0.2158	1.75	0.2173	0.42	0.2167	0.96
$R_c$	$0.1715 \pm 0.0056$	0.1723	-0.14	0.1707	0.14	0.1709	0.12
$A_{FB}^b$	$0.0979 \pm 0.0023$	0.1020	-1.77	0.1030	-2.22	0.1030	-2.19
$A_{FB}^c$	$0.07351 \pm 0.0048$	0.0729	0.12	0.0736	-0.01	0.0735	0.01
$\mathcal{A}_b$	$0.863 \pm 0.049$	0.933	-1.45	0.935	-1.49	0.936	-1.50
$\mathcal{A}_c$	$0.625 \pm 0.084$	0.667	-0.50	0.668	-0.51	0.668	-0.51
$\mathcal{A}_\tau$	$0.1401 \pm 0.0067$	0.1457	-0.83	0.1469	-1.01	0.1464	-0.95
$\mathcal{A}_e$	$0.1382 \pm 0.0076$	0.1457	-0.99	0.1469	-1.14	0.1467	-1.12
$\sin^2 \Theta_{eff}^{lept} \langle Q_{FB} \rangle$	$0.2320 \pm 0.0010$	0.2317	0.31	0.2315	0.46	0.2316	0.44
$M_W$ [GeV]	$80.356 \pm 0.125$	80.353	0.03	80.401	-0.36	80.425	-0.55
$1 - M_W^2/M_Z^2$	$0.2244 \pm 0.0042$	0.2235	0.21	0.2226	0.44	0.2221	0.55
$m_t$ [GeV]	$175 \pm 6.$	172.2	0.46	172.3	0.46	171.9	0.514
$\sin^2 \Theta_{eff}^{lept}(A_{LR})$	$0.23061 \pm 0.00047$	0.2317	-2.16	0.2315	-1.86	0.2316	-1.89

Table 2: Measurements[10] and the predicted results of the fits with minimum  $\chi^2$ . The pulls are defined by (measurement - predicted value) / error of the measurement.

of the chargino masses on the parameter  $\mu$  in a region of the parameter space which yields a good global  $\chi^2$ . In case of high  $\tan\beta$ ,  $m_{\tilde{\chi}_2}$  is almost symmetric around zero, whereas in case of low  $\tan\beta$  this dependence is more complicated, as can be seen from fig. 4. For  $M_2 = 3 |\mu|$  the light chargino mass passes zero at  $\mu = -40$  GeV, so the following low  $\tan\beta$  plots were made for  $\mu > -40$  GeV and  $\mu \leq -40$  GeV. The asymmetric structure of fig. 4 is reflected in the contours of constant  $R_b$  in the  $m_{\tilde{\chi}_2}$  versus light scalar top  $m_{\tilde{t}_2}$  plane (see fig. 6). High values of  $R_b$  up to 0.2194 are possible (see figs. 6 and 7), although these special regions of the parameter space are already experimentally excluded by the lower limits on sparticle masses.

Taking  $M_2 = |\mu|$  does not change these results very much, as can be seen from a comparison of the  $\chi^2$  distributions in fig. 8 ( $M_2 = 3 |\mu|$ ) and fig. 9 ( $M_2 = |\mu|$ ). The small increase of the  $\chi^2$  at chargino masses around 80 GeV in the left hand part of fig. 9 is due to neutralino threshold singularities, for which an additional  $\chi^2$  contribution has been added, if the sum of two neutralino masses is close to the  $Z^0$  mass. The sharp increase of the  $\chi^2$  function at low chargino masses is due to experimental limits on chargino, neutralino and stop masses from LEP 1.5 [15, 16, 17].

## 4.2 Optimization of Parameters

An optimization of free parameters of the MSSM was performed by minimizing a  $\chi^2$  function using MINUIT [22]. Several contributions to the  $\chi^2$  were taken into account:

- experimental limits on the masses of supersymmetric particles and neutralino production from LEP 1.5 and Tevatron [15, 16, 17]
- precision measurements of on resonance observables from LEP [10], taking error correlations into account
- the measurement of the branching ratio  $\frac{BR(b \rightarrow s\gamma)}{BR(b \rightarrow ce\bar{\nu})}$  from CLEO [14]

The experimental limits included in the fit are summarized in table 1 [1, 15, 16, 17, 18, 19]. The calculation of the total decay width of the Z boson into neutralinos is based on reference [33], the calculation of the ratio  $b \rightarrow s\gamma$  on reference [34].

As already mentioned,  $R_b$  mainly depends on the stop mass and the light chargino mass for the low  $\tan\beta$  and on the pseudoscalar Higgs mass and chargino mass for the high  $\tan\beta$  scenario. In order to get a feeling for the size of the effects, the dependence of the  $\chi^2$  function on these masses is studied first for the low and the high  $\tan\beta$  solutions, respectively. The best solutions will be presented in the next chapter.

#### 4.2.1 Low $\tan\beta$ scenario

Fig. 10 shows the change in the best obtainable  $\chi^2$  in the chargino - stop plane. For each value of the lighter scalar top  $m_{\tilde{t}_2}$  and lighter chargino  $m_{\tilde{\chi}_2^\pm}$  in a grid of  $10 \times 10$  points an optimization of  $m_t$ ,  $\alpha_s$  and the stop mixing angle  $\Phi_{mix}$  was performed, assuming  $M_2 = 3 |\mu|$  for a fixed value of  $\tan\beta = 1.6$ . In the next section this assumption on  $M_2$  will be dropped. Low sparticle masses yield a sharp increase in the  $\Delta\chi^2$  in fig. 10 because of the included mass limits. The minimum  $\chi^2$  is obtained for chargino masses just above the experimental limit, although it increases only slowly with increasing sparticle masses.  $R_b$  increases significantly with decreasing values of the stop and chargino mass, as can be seen from fig. 11. Much less significant is the change of  $R_c$ . Within the plane of fig. 11 it changes less than 0.0005 units. The increase of  $R_b$  must be compensated by a decrease of  $\alpha_s$  (see fig. 12) in order to keep the total Z-width constant. The stop mixing angle  $\Phi_{mix}$ , shown in fig. 13, is mainly determined by the CLEO measurement of  $b \rightarrow s\gamma$ . The chargino contribution to  $b \rightarrow s\gamma$  is proportional to the Higgs mixing parameter  $\mu$ , which changes its sign for  $m_{\tilde{\chi}^\pm} \approx 60$  GeV (see fig.4), so the  $b \rightarrow s\gamma$  rate changes rapidly for these chargino masses, as shown in fig. 14. The uncertainty in the predicted  $b \rightarrow s\gamma$  rate from the renormalization scale has been taken into account and was varied between  $m_b/2$  and  $2m_b$  [35]. The scale itself has been chosen to be  $m_b$ .

#### 4.2.2 High $\tan\beta$ scenario

Similar fits can be performed for the high  $\tan\beta$  scenario in the pseudoscalar Higgs  $m_A$  versus light chargino plane. In fig. 15 the resulting change in the  $\chi^2$  is given for fixed  $\tan\beta = 50$ . For small chargino masses there is a sharp increase in the  $\chi^2$  due to the corresponding mass limit, see above. The highest values for  $R_b$  can be obtained for small values of  $m_A$  and  $m_{\tilde{\chi}^\pm}$ , see fig. 16. As in the low  $\tan\beta$  case the enhancement of  $R_b$  must be compensated by a decrease of  $\alpha_s$ , see fig. 17, and the change of  $R_c$  is small, less than 0.0006 within the given parameter plane. The mixing angle, shown in fig. 18, is mainly determined by the  $b \rightarrow s\gamma$  rate, which can be fitted in the whole  $m_A - \chi^\pm$  plane, see fig. 19.

### 4.3 Best Solutions

#### *Standard Model Fits:*

The input values from  $M_W$ ,  $m_t$ , the electroweak mixing angle and the  $Z^0$  line shape observables have been summarized in table 2. The fine structure constant was taken to be  $1/\alpha = 128.89 \pm 0.09$ [38]. The SM predictions were obtained from the ZFITTER package [20] and all the error correlations were taken from [10]. The fits were made with  $\alpha_s$ ,  $m_t$  and  $m_H$  as free parameters, which resulted in

$$\begin{aligned}\alpha_s(M_Z) &= 0.1201 \pm 0.0032 \\ m_t &= 172.2_{-5.7}^{+5.8} \text{ GeV} \\ m_H &= 146_{-68}^{+112} \text{ GeV} \\ \sin^2 \theta_{\overline{MS}} &= 0.2317 \pm 0.0004.\end{aligned}$$

Both the strong coupling constant and the electroweak mixing angle  $\sin^2 \theta_{\overline{MS}}$ , which can be calculated from the other parameters, have been determined at the scale  $M_Z$  in the  $\overline{MS}$  renormalization scheme. The quoted errors have been determined using MINOS [22]. Further details of the procedure are described elsewhere, see for example [36, 37, 39]. The  $\chi^2/d.o.f$  of the SM fit is 18.5/15 which corresponds to a probability of 24%. Here, the main contributions to the  $\chi^2$  originate from  $\sin^2 \Theta_{eff}^{lept}$  from SLD ( $\Delta\chi^2 = 4.7$ ),  $R_b$  ( $\Delta\chi^2 = 3.1$ ) and  $A_{FB}^b$  ( $\Delta\chi^2 = 3.1$ ). The prediction of  $R_c$  is good. The correlation parameter between  $m_H$  and  $m_t$  for the best fit is approximately 0.7; this strong correlation is shown in fig. 20. One observes that the upper limit on the Higgs mass is obtained for  $m_t$  above 175 GeV; however, the upper limit is sensitive to  $\sin^2 \Theta_{eff}^{lept}$  as shown by the dashed contour in fig. 20, where the precise value of  $\sin^2 \Theta_{eff}^{lept}$  from SLD was excluded from the fit. The dependence of  $\sin^2 \Theta_{eff}^{lept}$  on the SM Higgs mass is approximately logarithmic (see fig. 21). The LEP data alone without SLD yields  $m_H = 250_{-112}^{+187}$  GeV, SLD alone yields  $m_H = 15_{-8}^{+25}$  GeV, as indicated by the squares in fig. 21. The latter value is excluded by the lower limit of 58.4 GeV from the combined LEP experiments [19]. In addition, the ALEPH Collaboration gives a recent limit of 63.9 GeV on the SM Higgs mass [18]. The  $\Delta\chi^2$  dependence of the Higgs mass is shown in fig. 22 for various conditions.

#### *MSSM Fits and Comparison with the SM:*

In order to obtain the best MSSM fits the assumption  $M_2 = 3 |\mu|$  is dropped and  $M_2$  is treated as a free parameter.  $R_b$  increases with decreasing  $\tan\beta$ , but the  $b \rightarrow s\gamma$  rate becomes too small if  $\tan\beta$  is near one. With  $b \rightarrow s\gamma$  included in the fit and a free  $\tan\beta$ , the preferred value of  $\tan\beta$  was either around 1.6 or 34.

The fit results for these values of  $\tan\beta$  are given in table 3 and the predicted values of all observables with their pulls have been summarized in table 2. Note that the MSSM prediction of the W-boson mass is always higher than the Standard Model one, but the values of the strong coupling constant, the electroweak mixing angle and the top mass are very similar in the MSSM

$$\begin{aligned}\alpha_s(M_Z) &= 0.116 \pm 0.005 \\ m_t &= 172 \pm 5 \text{ GeV} \\ \sin^2 \theta_{\overline{MS}} &= 0.2315 \pm 0.0004.\end{aligned}$$

These values are for the low  $\tan\beta$  scenario, but for high  $\tan\beta$  the same values are obtained, except for  $\alpha_s = 0.119 \pm 0.005$  in that case. The remaining parameters are given in table 3. The Higgs mass is not an independent parameter in the MSSM, since the couplings in the Higgs potential are gauge couplings, which limit the mass of the lightest Higgs to a rather narrow range[39]. The high  $\tan\beta$  needs a light pseudoscalar Higgs mass. Since the lightest Higgs mass is strongly correlated with the pseudoscalar Higgs mass, it is low too.

For the best solutions the gluino mass was fixed to 1500 GeV, the stau mass to 500 GeV and the sbottom mass to 1000 GeV in both the low and the high  $\tan\beta$  scenario, since they are less sensitive to the LEP observables and therefore cannot be fitted. Their influence was studied by fixing them to different values and repeating the fits again. First the low  $\tan\beta$  scenario will be discussed. A variation of the gluino mass from 200 GeV up to 2000 GeV did not change the best obtainable  $\chi^2$ , varying the stau mass in the same range changed the  $\chi^2$  less than 0.2. Furthermore, the best obtainable  $\chi^2$  changed less than 0.2 when varying the sbottom mass and pseudoscalar Higgs mass from 800 GeV to 2000 GeV. For values of these two parameters below 800 GeV the  $\chi^2$  increased significantly, mainly because the prediction of  $R_b$  became too small.

Within the high  $\tan\beta$  scenario no significant change of the global  $\chi^2$  was detected when the gluino mass was varied between 200 GeV and 2000 GeV, but the stau mass was somewhat more sensitive. A variation of this parameter between 300 GeV and 700 GeV changed the global  $\chi^2$  less than 0.2, but if it was chosen higher than 1000 GeV the  $\chi^2$  increased up to 1.6 units, mainly because the prediction of  $\mathcal{A}_\tau$  became worse. The sbottom mass was varied between 800 GeV and 2000 GeV. As in the low  $\tan\beta$  case there was no dependence on this parameter if it was chosen heavy, but for low values the preferred top mass became too small.  $M_2$  was fixed at 1500 GeV. A variation between 1000 GeV and 2000 GeV changed the best reachable  $\chi^2$  less than 0.2, for smaller values the global  $\chi^2$  increased up to one unit. Note that  $\tan\beta$  was left as a free parameter in this case.

To check the influence of the assumptions on  $M_1$  for the best fits, the GUT relation  $M_1 = 5/3 \tan^2 \theta_W M_2$  was dropped and the fit was repeated with a free  $M_1$ , but this did not improve the best obtainable  $\chi^2$  significantly.

A direct comparison to the Standard Model fits is given in figs. 24-25. The resulting Standard Model  $\chi^2/d.o.f. = 18.5/15$  corresponds to a probability of 24%, the MSSM fits correspond to probabilities of 19% ( $\tan\beta = 1.6$ ,  $\chi^2/d.o.f. = 16.1/12$ ) and 9% ( $\tan\beta=34$ ,  $\chi^2/d.o.f. = 17.7/11$ ). In counting the d.o.f the insensitive (and fixed) parameters were ignored. Although the global  $\chi^2$  of the fits can be improved and the remaining discrepancy in  $R_b$  can be fully explained if Supersymmetry is assumed, both the high and the low  $\tan\beta$  scenario have a lower probability than the SM, because of the larger number of free parameters in MSSM. Therefore, from the point of view of electroweak precision measurements there is no compelling need for Supersymmetrie.

Another interesting point is the fitted value of  $\alpha_s(M_Z)$ . In previous analysis with the high values of  $R_b$   $\alpha_s(M_Z)$  in the MSSM ( $\approx 0.11$ ) was always significantly smaller than the SM value ( $0.123 \pm 0.005$ [19]), which supported the low energy values from deep inelastic scattering (DIS) ( $0.112 \pm 0.005$ [19]) and lattice calculations of the heavy quark splittings ( $0.110 \pm 0.006$ [19]). However, the discrepancies between the low energy  $\alpha_s$  values and the LEP data have practically disappeared at the Warsaw Conference[40]: the Standard Model value ( $0.120 \pm 0.003$ , see above) is now in agreement with DIS measurements ( $0.115 \pm 0.005$ [40]), lattice calculations  $0.117 \pm 0.003$ [40] and the world average  $0.118 \pm 0.003$ [40]. The MSSM values of  $\alpha_s$  are in good agreement with these other determinations, as shown in fig. 26.

## 4.4 Discovery Potential at LEP II

The particle spectrum for the best fits, as shown in table 3, suggests that some SUSY particles could be within reach of LEP II. If they are not found, LEP II will provide stringent SUSY mass limits[37, 39]. In the following the consequences of increased mass limits on the fits are discussed for both the low and high  $\tan\beta$  scenario.

### *Chargino Searches:*

The  $\chi^2$  in the region of the best low  $\tan\beta$  fit increases slowly for increasing chargino masses, see fig. 23. Chargino masses above a possible LEP II limit of 95 GeV will increase the global  $\chi^2$  of the fit by approximately 2 units, which decreases the probability from 19 to 11%. For the high  $\tan\beta$  scenario the dependence of the global  $\chi^2$  on the chargino mass is small, see fig.15, so increased limits will hardly change the probability of about 9% for the best possible fit in this scenario.

### *Stop and Neutralino Searches:*

The best  $\tan\beta = 1.6$  fit has a light stop mass of about 49 GeV, and the lightest neutralino is about 55 GeV, so this solution is not excluded by stop searches at LEP1 and the Tevatron [17]: LEP I limits for light right handed stops are about 45 GeV, while D0 limits exclude  $52(70) \text{ GeV} < m_{\tilde{t}_2} < 92(87) \text{ GeV}$  for  $m_{\tilde{\chi}_0} = 20(40) \text{ GeV}$ . Both limits hold only for neutralino masses less than 45 GeV.

The stop mass in the high  $\tan\beta$  solution is 238 GeV, and the lightest neutralino is quite heavy, above 100 GeV, so there is no conflict with stop searches.

### *Higgs Searches:*

The mass of the light scalar Higgs is a sensitive function of the top mass. If the top mass is below 180 GeV, the Higgs mass for the low  $\tan\beta$  fit should be observable at LEP II, especially if one includes the second order corrections, which will lower the Higgs mass by 10 - 15 GeV [39]. Within the high  $\tan\beta$  scenario both neutral Higgs bosons are light and have practically the same mass. This scenario can surely be excluded if no Higgses will be found at LEP 2.

## 5 CMSSM and $R_b$

In ref. [37] fits to low energy data have been performed within the constrained MSSM (CMSSM). In this case unification of gauge and b- $\tau$  Yukawa couplings is assumed. Reproducing the large mass splitting in the stop sector, as given in tab. 3, needs a very artificial fine tuning of the few free parameters of the CMSSM, especially for the trilinear and Yukawa coupling in the stop sector, which can drive the diagonal elements of the stop matrix, eq. 21, apart. Note that the off-diagonal elements of this matrix are too small to generate a large splitting, since the left-handed stop is considerably heavier than the top, implying that one of the diagonal elements is considerably larger than the off-diagonal elements. In addition, problems arise with electroweak symmetry breaking, since this requires  $\mu > M_2$ , while  $R_b$  requires  $\mu < M_2$  for a significant enhancement.

In conclusion, within the CMSSM the high value of  $R_b$  cannot be explained, so in this scenario the solution must be sought in systematic errors for the experiments, like background from the charm sector.

## 6 Conclusions

The MSSM provides a good description of all electroweak data, but because of the high number of free parameters in this Model, its description of recent electroweak data is worse than the SM one. With all mass bounds and the  $b \rightarrow s\gamma$  rate included in the fit, the best  $\chi^2/d.o.f$  in the MSSM is 16.1/12, which corresponds to a probability of 19% as compared to the SM probability of about 24%. The best MSSM fit with light stops and light charginos is obtained for  $\tan\beta = 1.6$ . Another solution with  $\tan\beta = 34$  and light Higgses has a probability of only 9%. Although the MSSM can fully explain the remaining deviation of  $R_b$  from the SM value, its probability is not better because of the larger number of free parameters.

Fitted SUSY parameters and masses		
Symbol	$\tan\beta=1.6$	$\tan\beta=34$
	$b \rightarrow s\gamma$ inc.	
$m_t$ [GeV]	$172\pm 5$	$172\pm 5$
$\alpha_s$	$0.116 \pm 0.005$	$0.1190\pm 0.005$
$M_2$ [GeV]	$116\pm 18$	-
$\mu$ [GeV]	$61\pm 33$	$112\pm 100$
$m_{\tilde{t}_2}$ [GeV]	$49\pm 11$	$232\pm 321$
$\phi_{mix}$	$-0.1838\pm 0.073$	$0.05\pm 0.11$
$m_A$ [GeV]	-	$50\pm 5$
Particle Spectrum		
$m_{\tilde{t}_1}$ [GeV]	$\approx 1$ TeV	
$m_{\tilde{t}_2}$ [GeV]	49	238
$m_{\tilde{q}}$ [GeV]	1 TeV	
$m_{\tilde{l}}$ [GeV]	0.5 TeV	
$m_{\tilde{\chi}_1^\pm}$ [GeV]	151	1504
$m_{\tilde{\chi}_2^\pm}$ [GeV]	85	112
$m_{\tilde{\chi}_1^0}$ [GeV]	55	109
$m_{\tilde{\chi}_2^0}$ [GeV]	66	116
$m_{\tilde{\chi}_3^0}$ [GeV]	101	716
$m_{\tilde{\chi}_4^0}$ [GeV]	152	1504
$m_h$ [GeV]	109	50
$m_H$ [GeV]	$\approx 1.5$ TeV	115
$m_A$ [GeV]	1.5 TeV	50
$m_{H^\pm}$ [GeV]	$\approx 1.5$ TeV	122
$M_W^\pm$ [GeV]	80.401	80.425
$\frac{BR(b\rightarrow s\gamma)}{BR(b\rightarrow ce\bar{\nu})}/10^{-4}$	2.42	2.33
$\chi^2/d.o.f.$	16.1/12	17.7/11
Probability	19%	9%

Table 3: Values of the fitted parameters (upper part) and corresponding mass spectrum (lower part). The errors on the parameters are parabolic ones. On the right hand side the results of the optimization for high  $\tan\beta$  are given. In this case  $\tan\beta$  was left free and resulted in  $\tan\beta \approx 34$ . The dashes indicate irrelevant parameters which were chosen high.

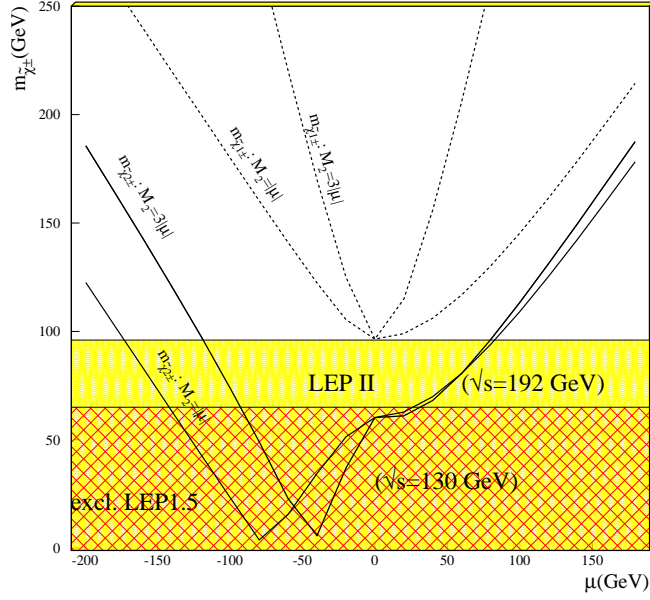


Figure 4: Dependence of the chargino masses on the parameter  $\mu$  for  $M_2 = |\mu|$  and  $M_2 = 3|\mu|$  for  $\tan\beta = 1.6$ ,  $\alpha_s \approx 0.117$  and  $\tilde{m}_{t_2} \approx 60$  GeV. No optimization of parameters was performed here. The shaded regions indicate chargino masses less than 65 GeV which are excluded by *LEP* 1.5 and chargino masses less than 96 GeV. It can be observed that for positive values of  $\mu$  two light charginos are easier to obtain, if  $\mu$  and  $M_2$  have similar values.

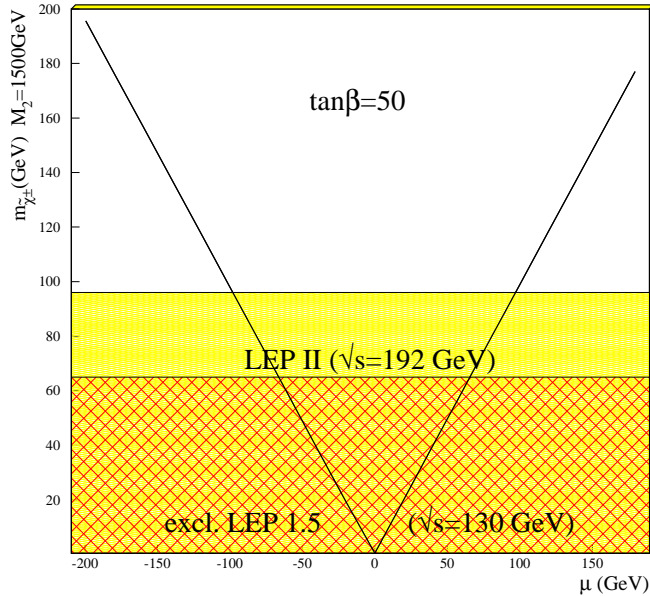


Figure 5: Dependence of the chargino masses on the parameter  $\mu$  for  $\tan\beta = 50$ . In this case  $M_2=1500$  GeV was used and no optimization of parameters was performed. The shaded regions indicate chargino masses less than 65 GeV which are excluded by *LEP* 1.5 and chargino masses less than 96 GeV, which is the discovery reach for *LEP* II. The light chargino mass is determined by  $\mu$ , whereas the heavy chargino mass is close to  $M_2 = 1500$  GeV. For a fixed given chargino mass there are two possible solutions corresponding to  $\mu < 0$  and  $\mu > 0$ , respectively.

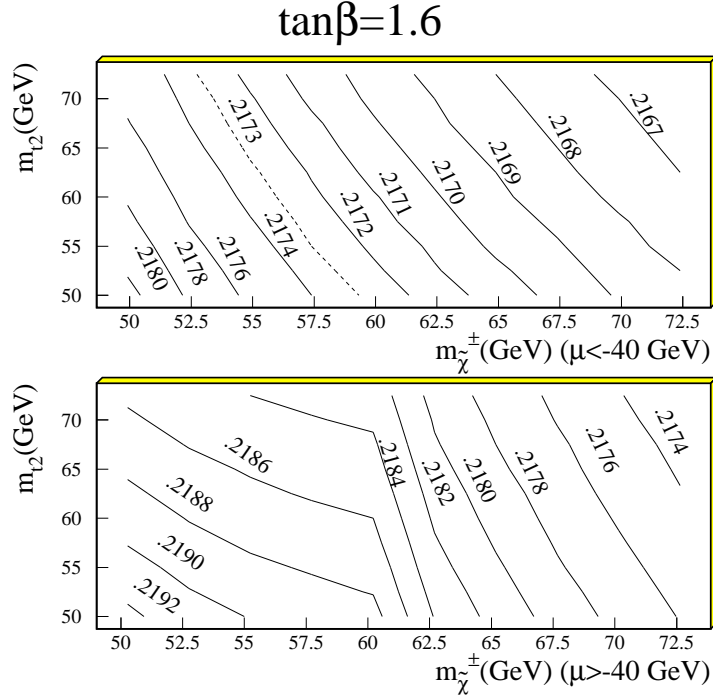


Figure 6:  $R_b$  in the light stop versus light chargino plane with  $M_2 = 3 |\mu|$  and  $\tan\beta = 1.6$ . The upper part shows the solution with  $\mu < -40$  GeV, in the lower part the one with  $\mu > -40$  GeV is displayed. In the latter solution quite high values for  $R_b$  are possible, as can be seen in the figure. The dashed line in the upper plot indicates the old  $2\sigma$  lower limit of  $R_b$ . Recent updates of electroweak data yield  $R_b = 0.2178 \pm 0.0011$ .

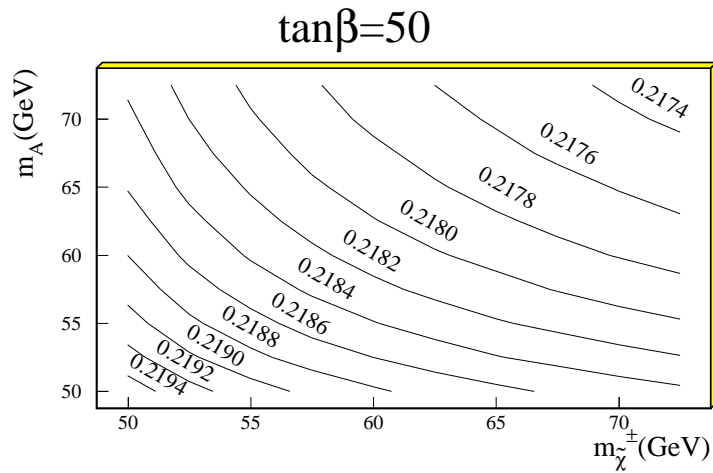


Figure 7:  $R_b$  in the  $m_A$  versus light chargino plane with  $M_2 = 3 |\mu|$  for the high  $\tan\beta$  solution.  $\mu$  was chosen positive here. In this case choosing the opposite sign for  $\mu$  doesn't change  $R_b$ .

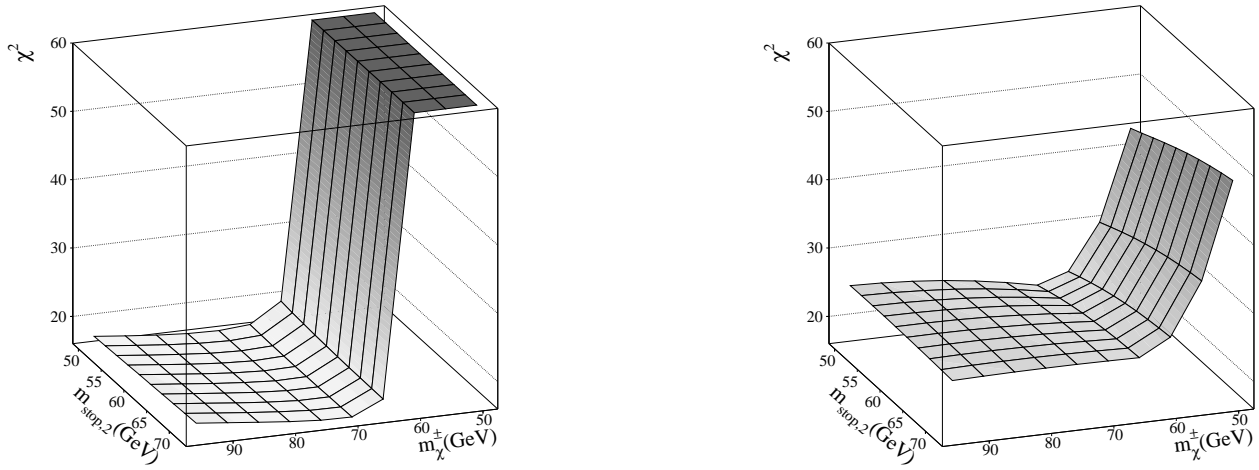


Figure 8: Dependence of the absolute  $\chi^2$  for  $\mu > -40$  GeV (left side) and  $\mu < -40$  GeV (right side), using  $M_2 = 3 |\mu|$ . No optimization of parameters was performed, but they were fixed to values near the minimum.

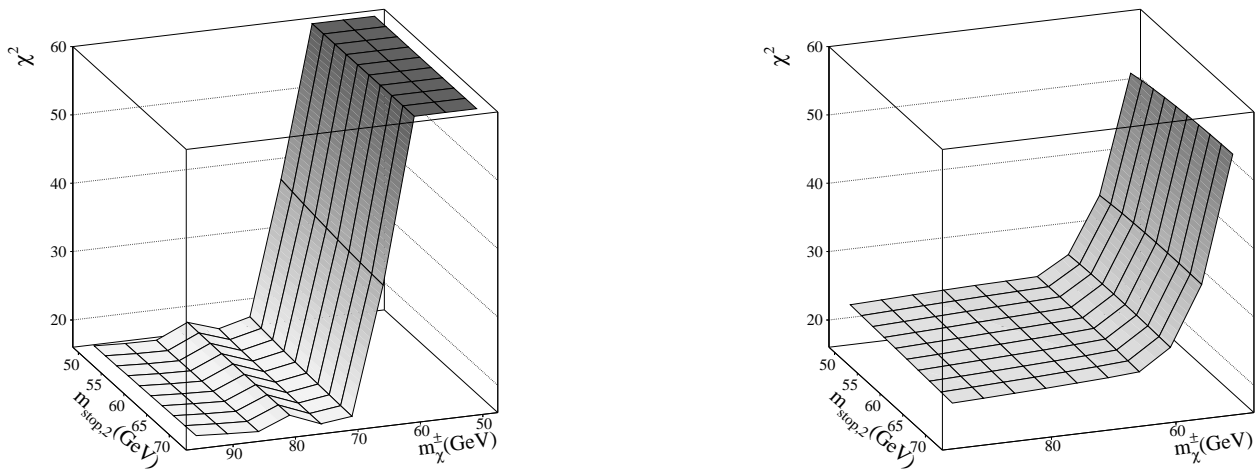


Figure 9: The same as 8, but for  $M_2 = |\mu|$ .

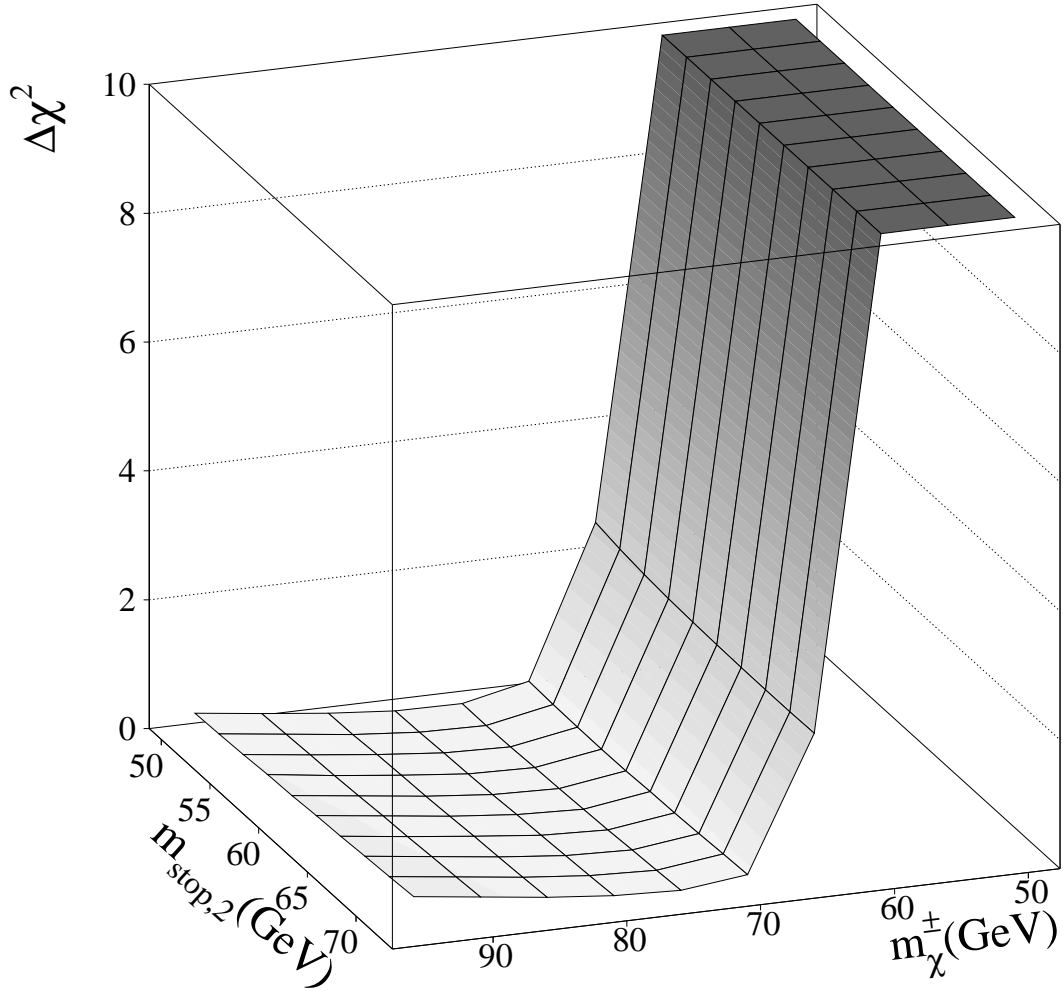


Figure 10: The  $\Delta\chi^2$  in the light stop and light chargino plane for  $\tan\beta = 1.6$ . At each point of the grid an optimization of  $m_t$ ,  $\alpha_s$  and the stop mixing angle  $\phi_{mix}$  was performed with  $\mu > -40$  GeV and  $M_2 = 3 |\mu|$ , including the ratio  $b \rightarrow s\gamma$ .

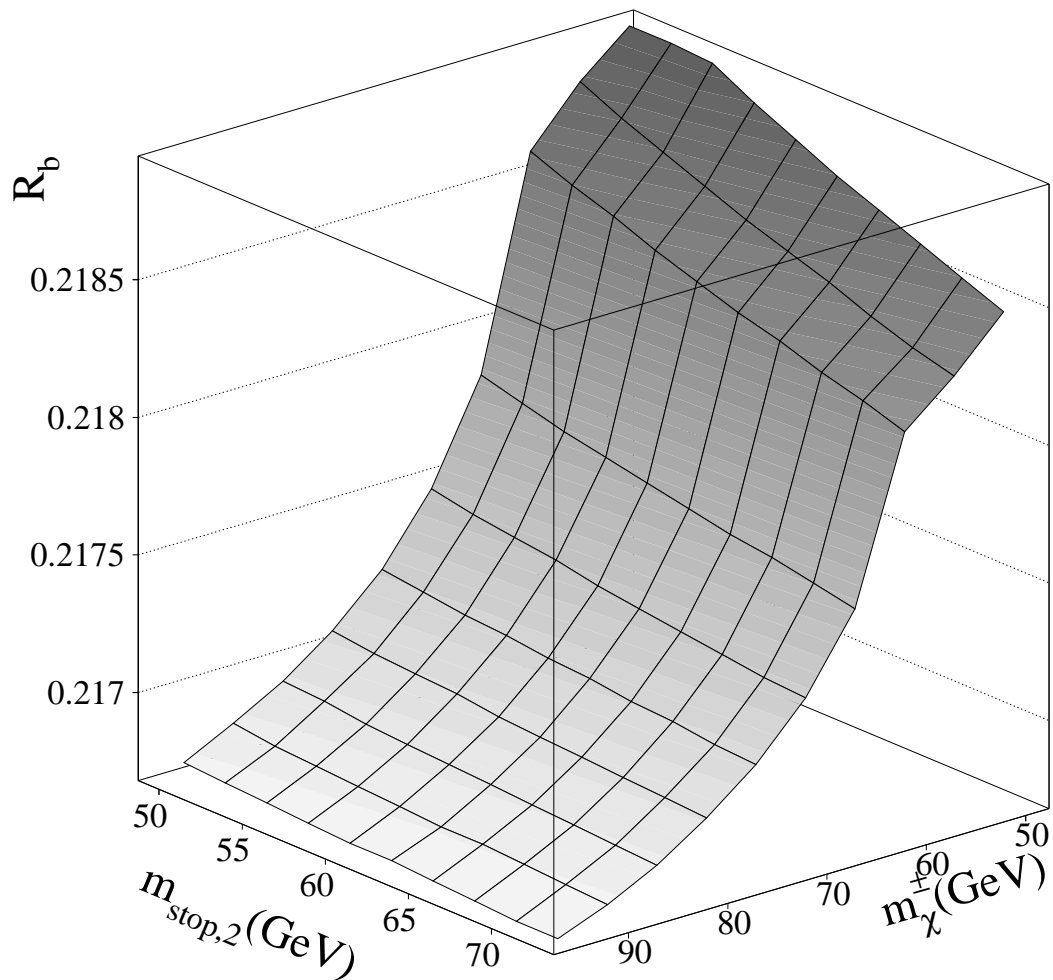


Figure 11:  $R_b$  in the light stop and light chargino plane. Optimization as in fig. 10.

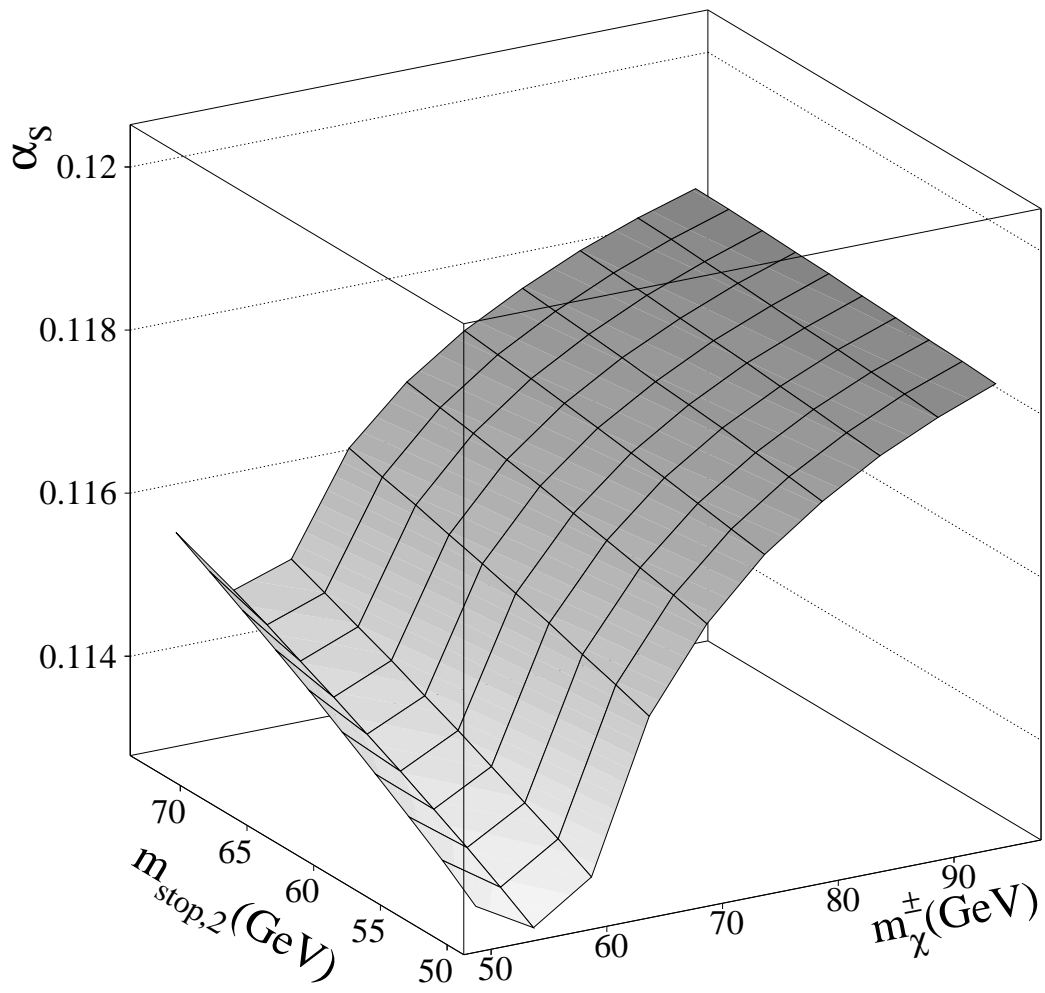


Figure 12:  $\alpha_s$  in the light stop and light chargino plane. Optimization as in fig. 10.

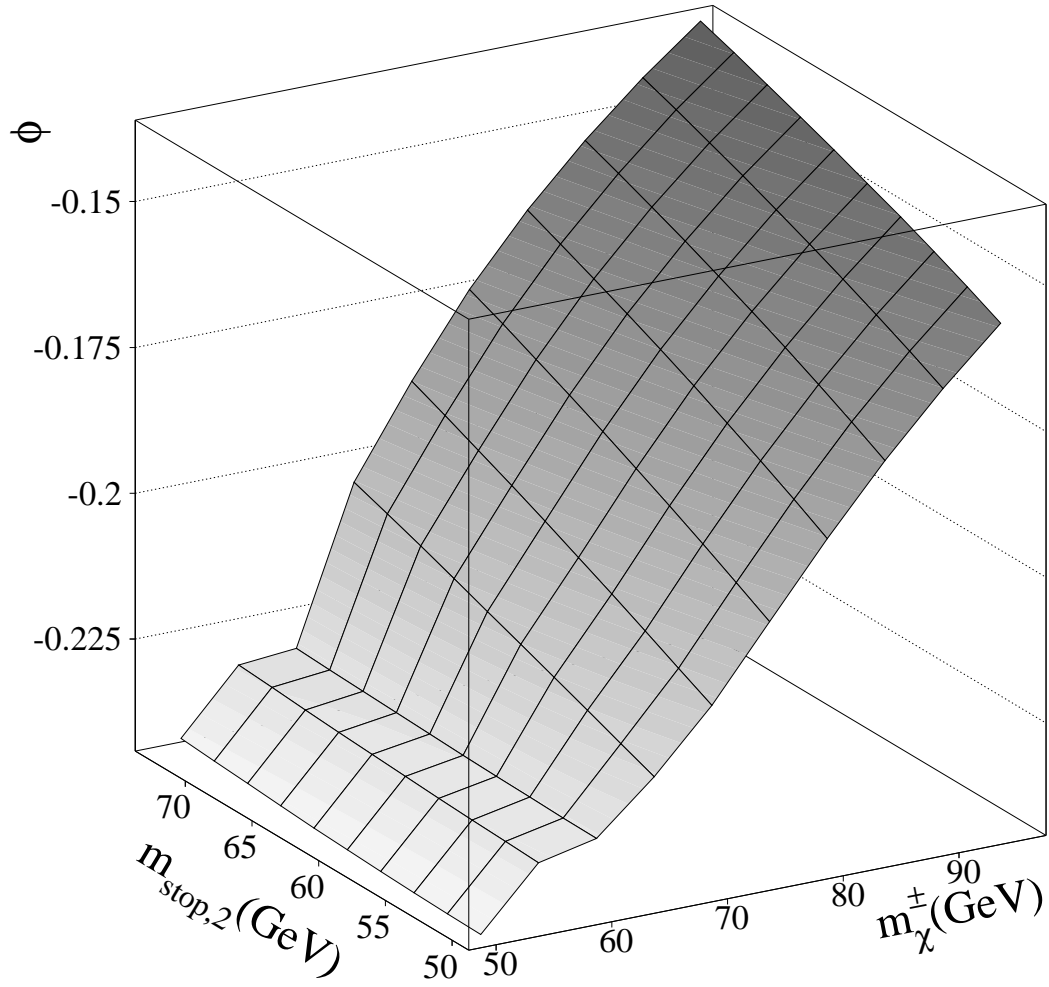


Figure 13: Stop mixing angle  $\phi_{mix}$  in the light stop and light chargino plane. It is mainly determined by the branching ratio  $b \rightarrow s\gamma$ . Optimization as in fig. 10.

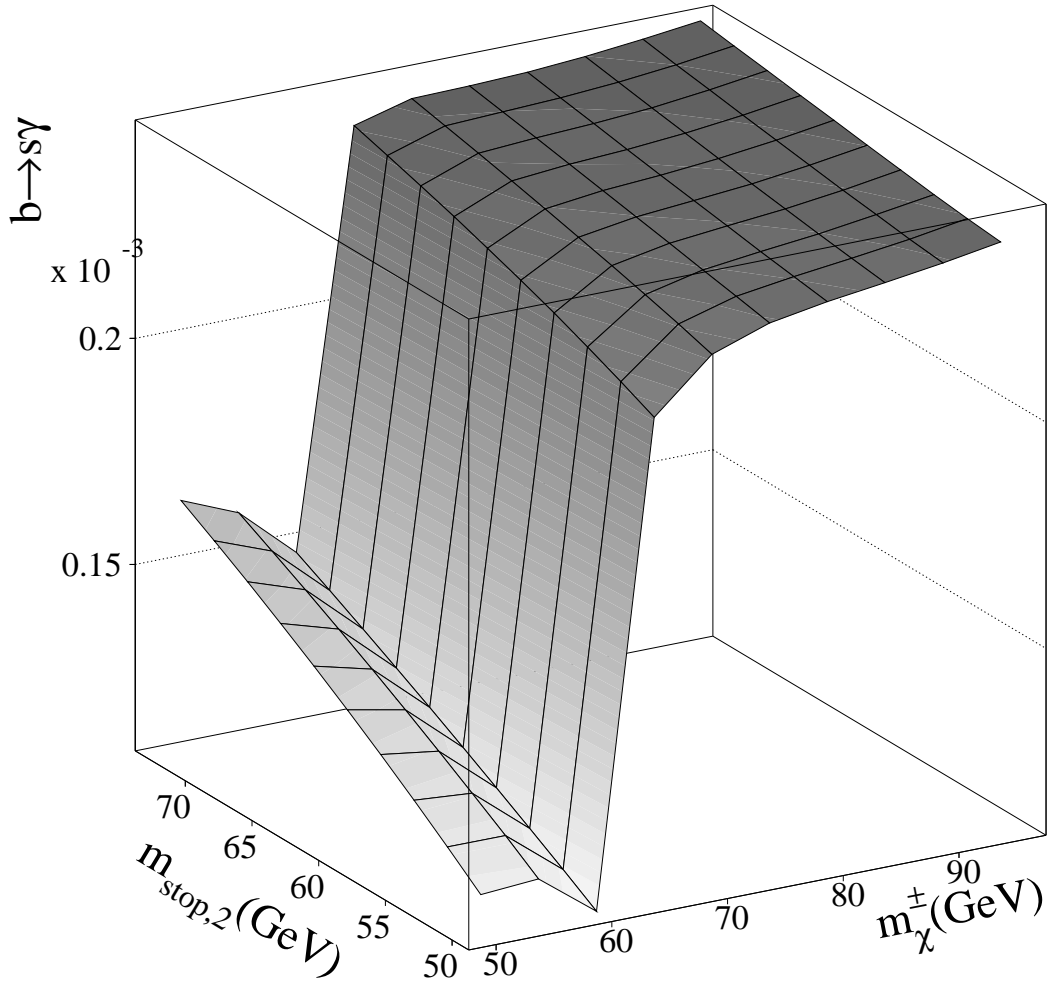


Figure 14:  $b \rightarrow s\gamma$  in the light stop and light chargino plane for  $\tan\beta = 1.6$ . For chargino masses higher than 60 GeV (and  $\mu > 0$ ) the predicted value is close to the CLEO measurement of  $2.32 \pm 0.67 \times 10^{-4}$ . Optimization as in fig. 10.

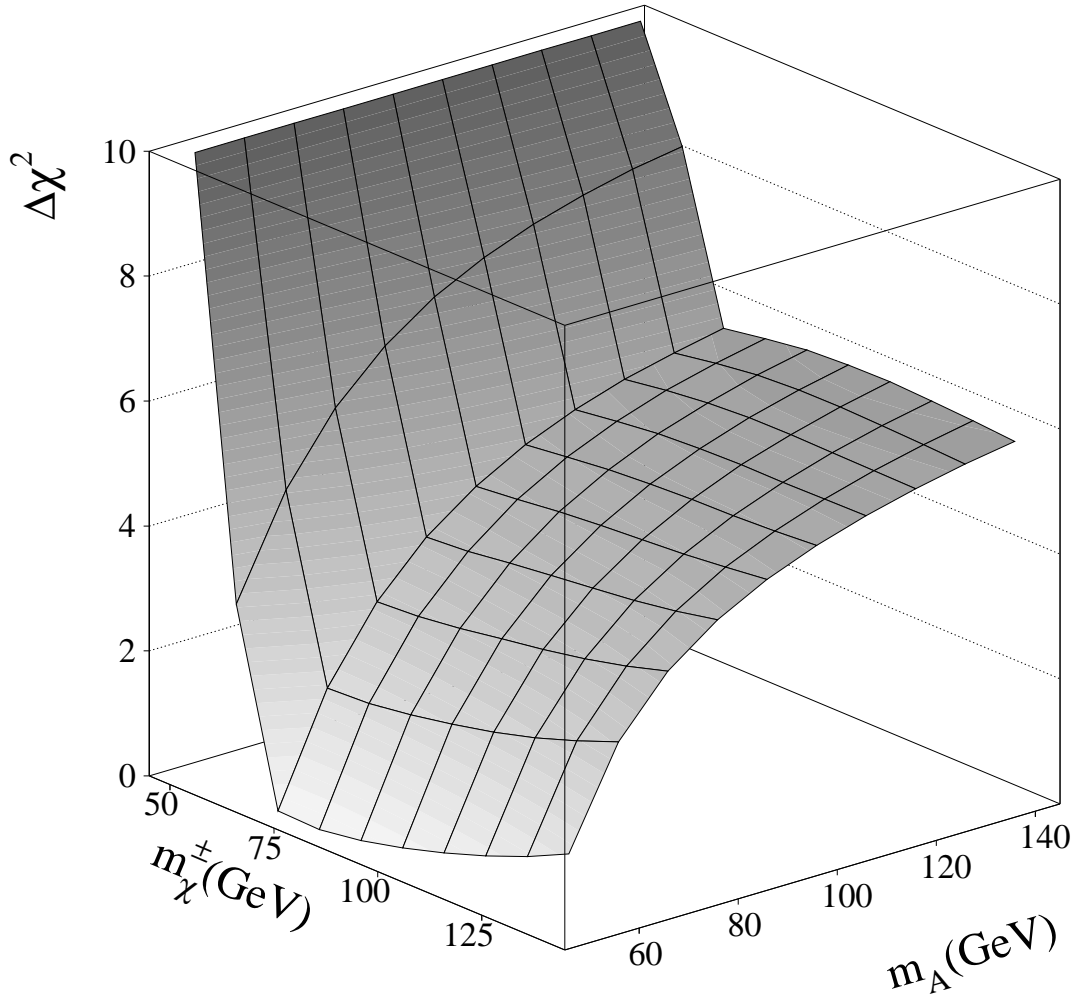


Figure 15: The  $\Delta\chi^2$  in the pseudoscalar Higgs and light chargino plane for  $\tan\beta = 50$ . For each given  $m_A$  and light chargino mass an optimization of  $m_t$ ,  $\alpha_s$ ,  $\tilde{m}_{t2}$  and the stop mixing angle  $\phi_{mix}$  was performed, including the  $b \rightarrow s\gamma$  rate. The irrelevant parameter  $M_2$  was set to 1500 GeV.

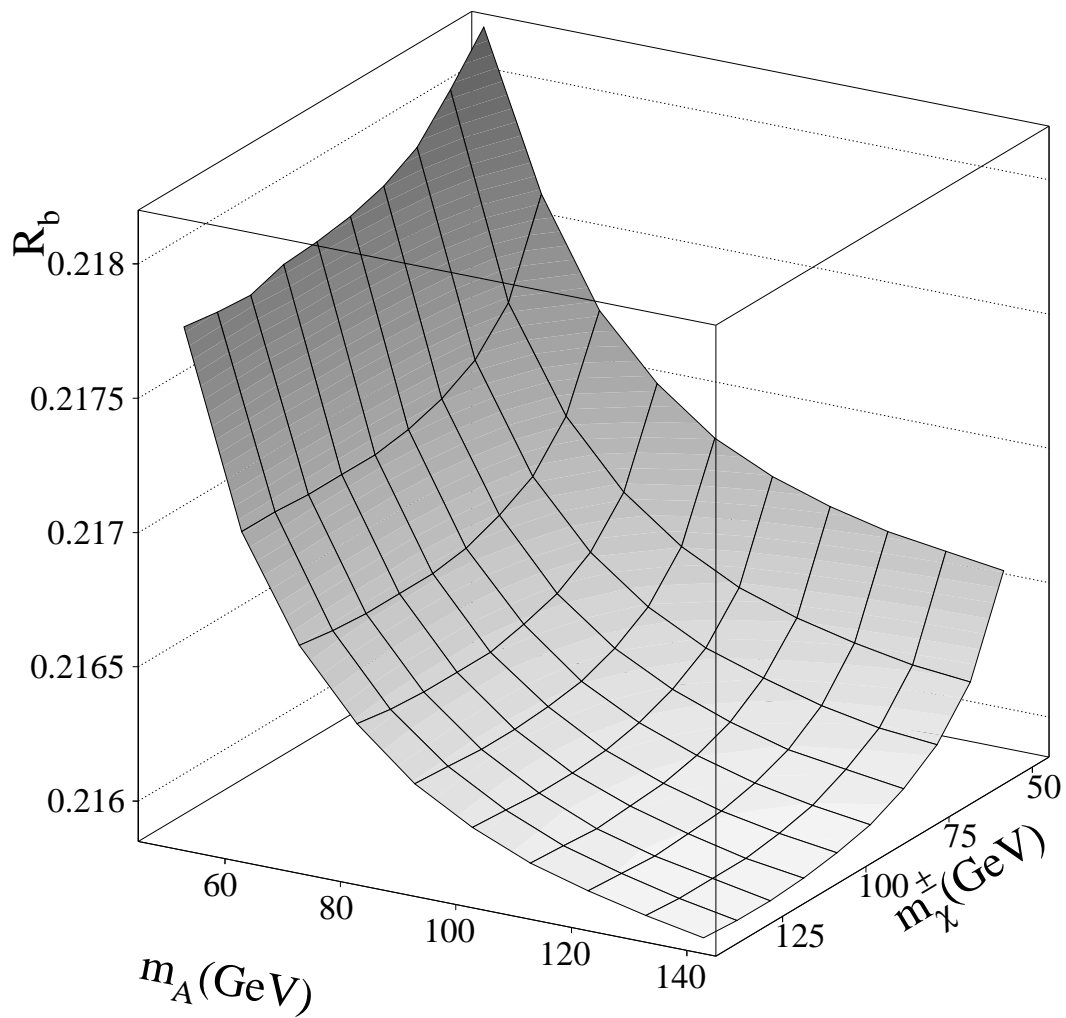


Figure 16:  $R_b$  in the pseudoscalar Higgs and light chargino plane for  $\tan \beta = 50$ . Optimization as in fig. 15.

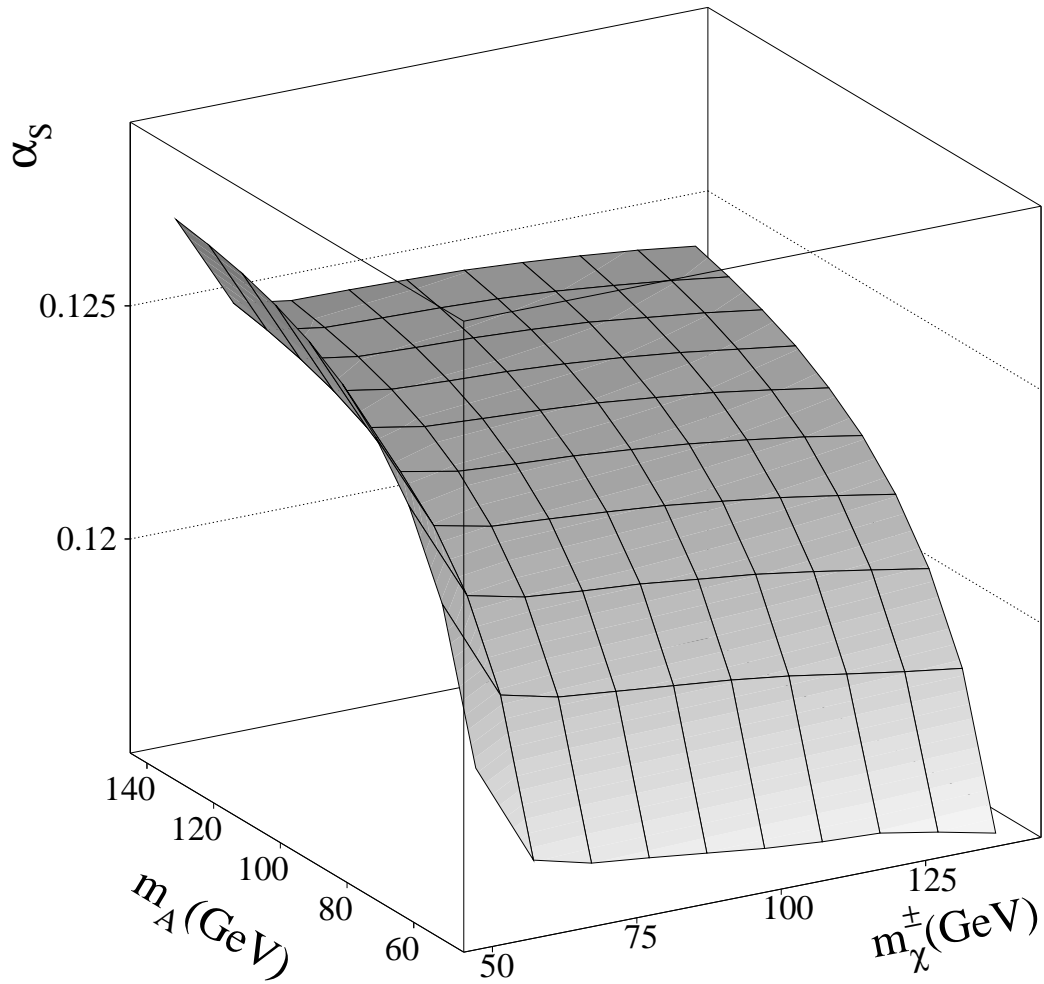


Figure 17:  $\alpha_s$  in the pseudoscalar Higgs and light chargino plane for  $\tan\beta = 50$ . Optimization as in fig. 15.

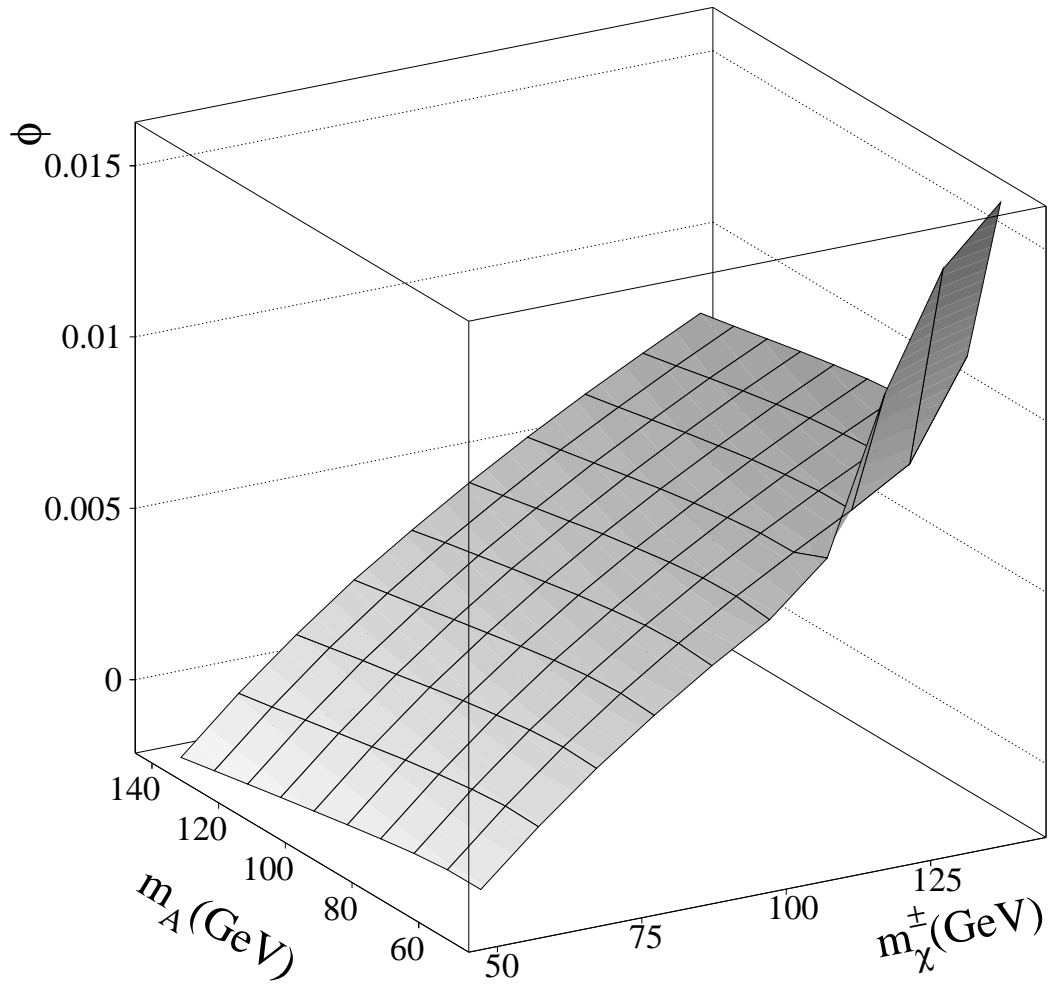


Figure 18: Stop mixing angle  $\phi_{mix}$  in the pseudoscalar Higgs and light chargino plane for  $\tan\beta = 50$ . Optimization as in fig. 15.

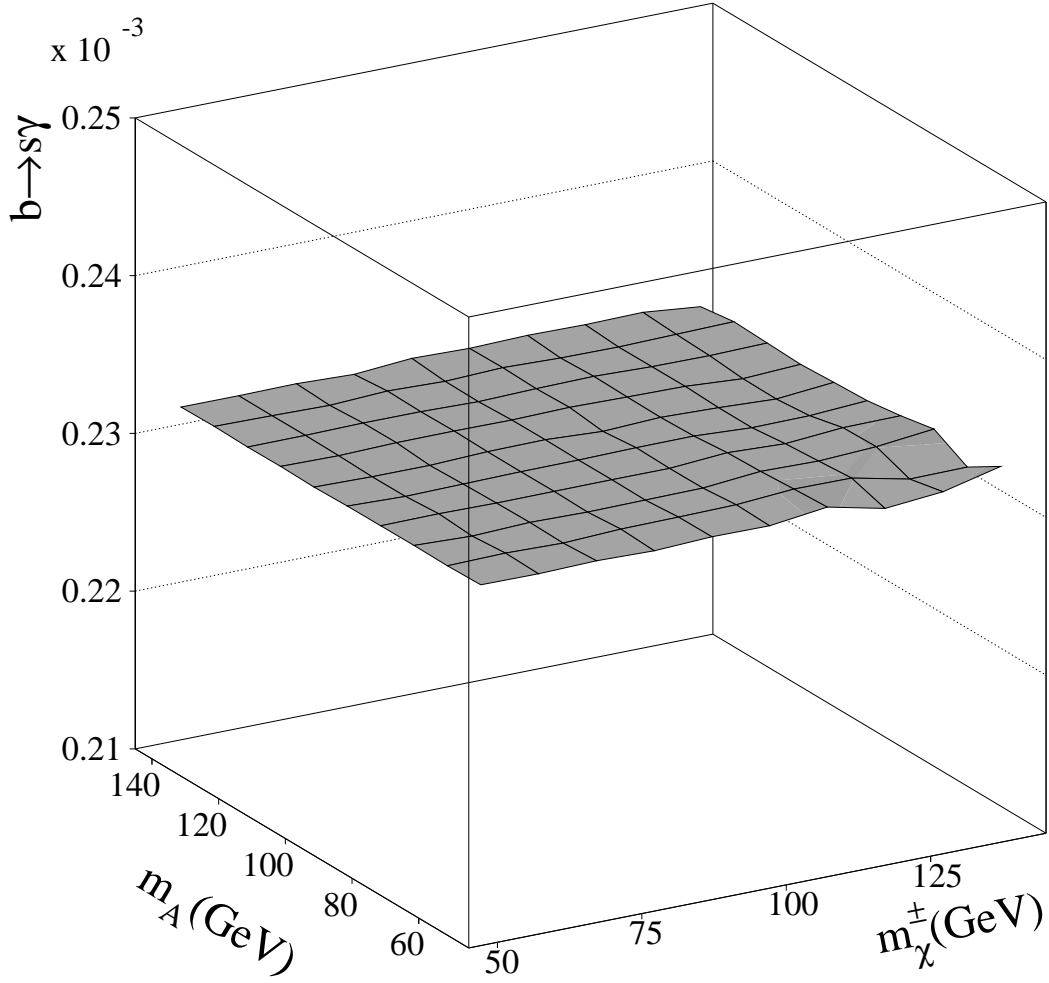


Figure 19:  $b \rightarrow s\gamma$  in the pseudoscalar Higgs and light chargino plane for  $\tan\beta = 50$ . The prediction is close to the CLEO measurement of  $2.32 \pm 0.67 \times 10^{-4}$  within the whole parameter space. Optimization as in fig. 15.

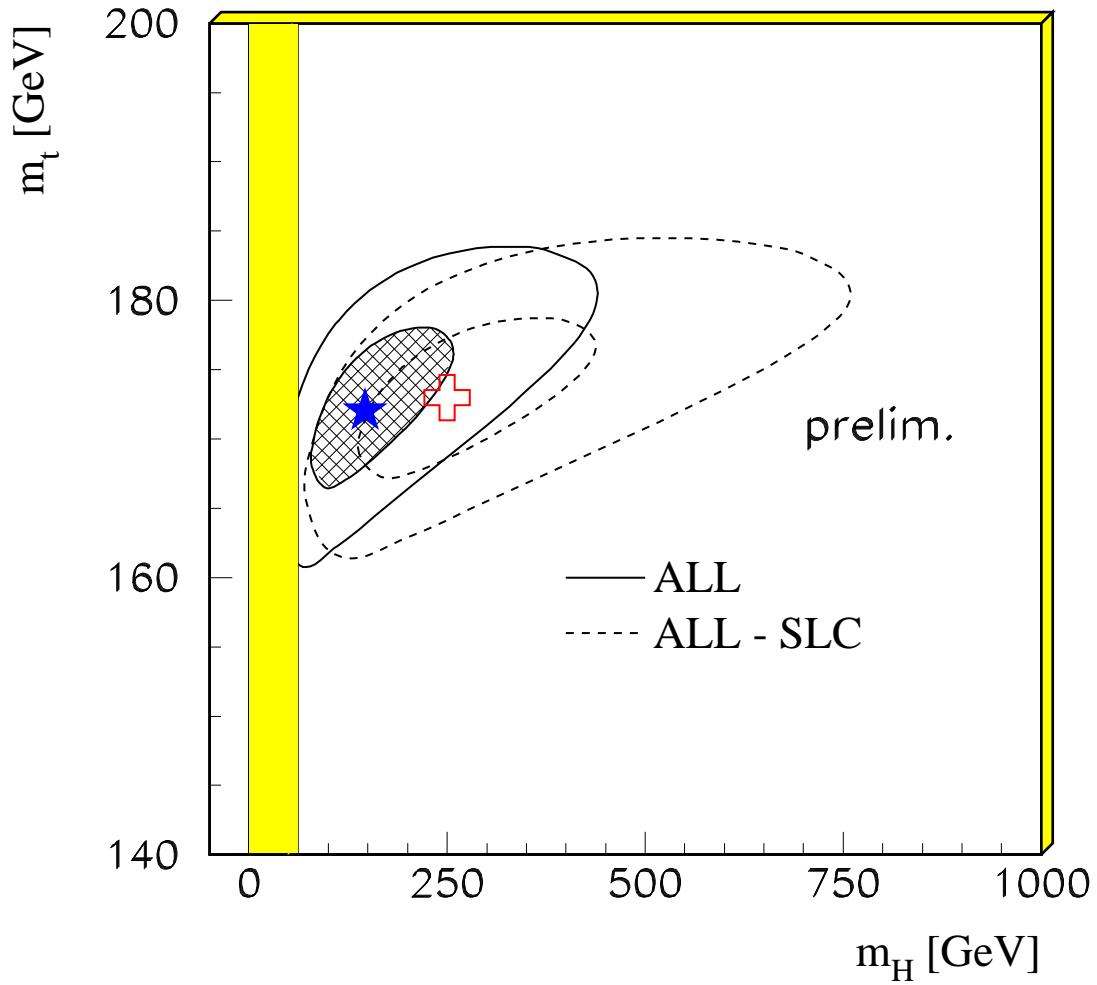


Figure 20:  $\Delta\chi^2 = 1$  and  $\Delta\chi^2 = 4$  contour lines for all electroweak data including  $\sin^2 \Theta_{eff}^{lept}$  from SLD (continuous line) and without it (dashed line). The stars indicate the best fits.

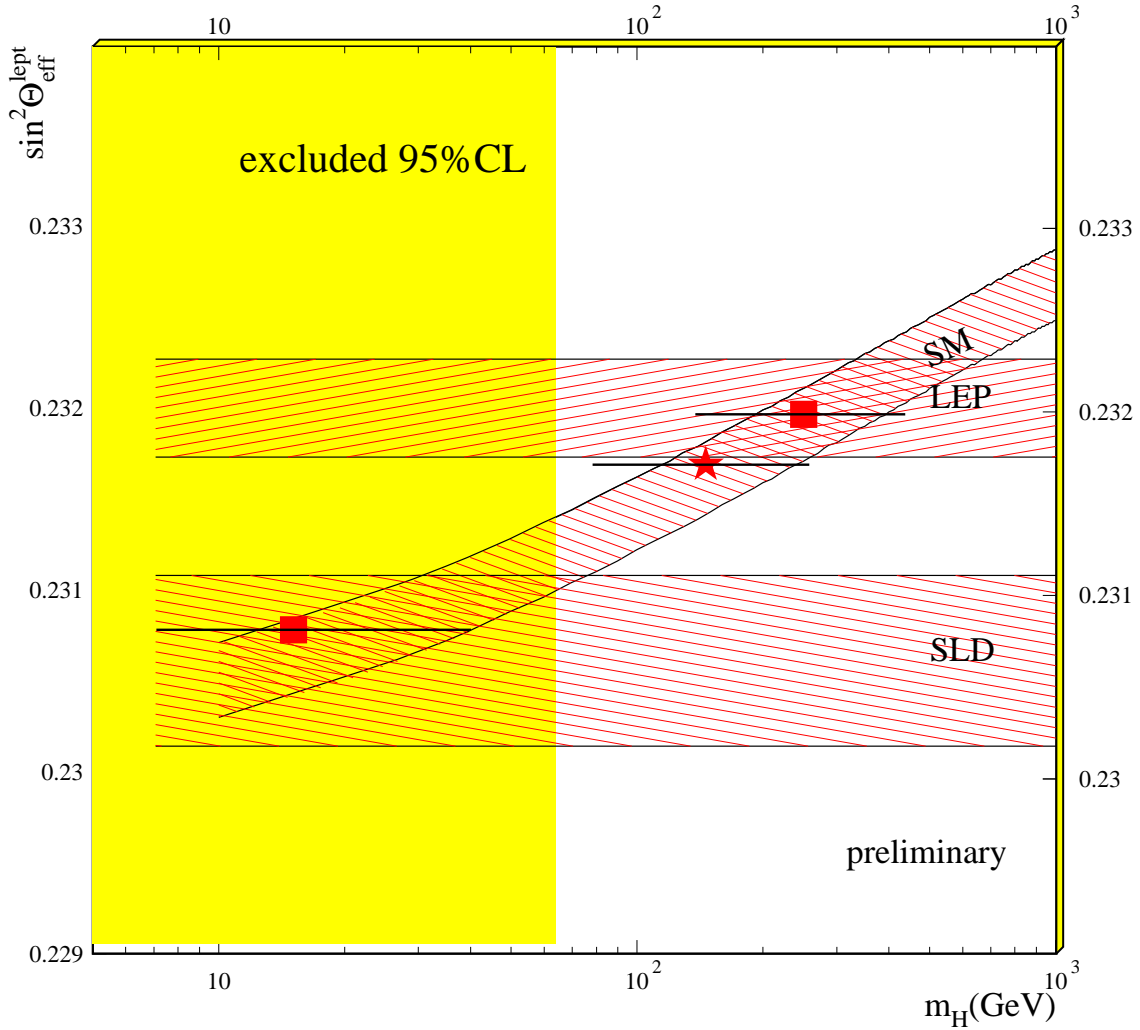


Figure 21: Dependence of the SM  $\sin^2 \Theta_{eff}^{lept}$  on the Higgs mass. The top mass  $m_t = 175 \pm 9$  GeV was varied within its error, as shown by the dashed band labelled SM (upper (lower) boundary  $m_t=166(184)$  GeV). The SLD and the LEP measurement of  $\sin^2 \Theta_{eff}^{lept}$  are also shown as horizontal bands. Fits to the electroweak data prefer  $m_t \approx 170$  GeV and light Higgs masses, as indicated by the squares for the separate LEP and SLD measurements, while the star is the result of the combined fit to SLD and LEP data. Clearly, the SLD value yields a Higgs mass less than the recent limits of 63.9 GeV by direct Higgs searches at LEP (shaded area).

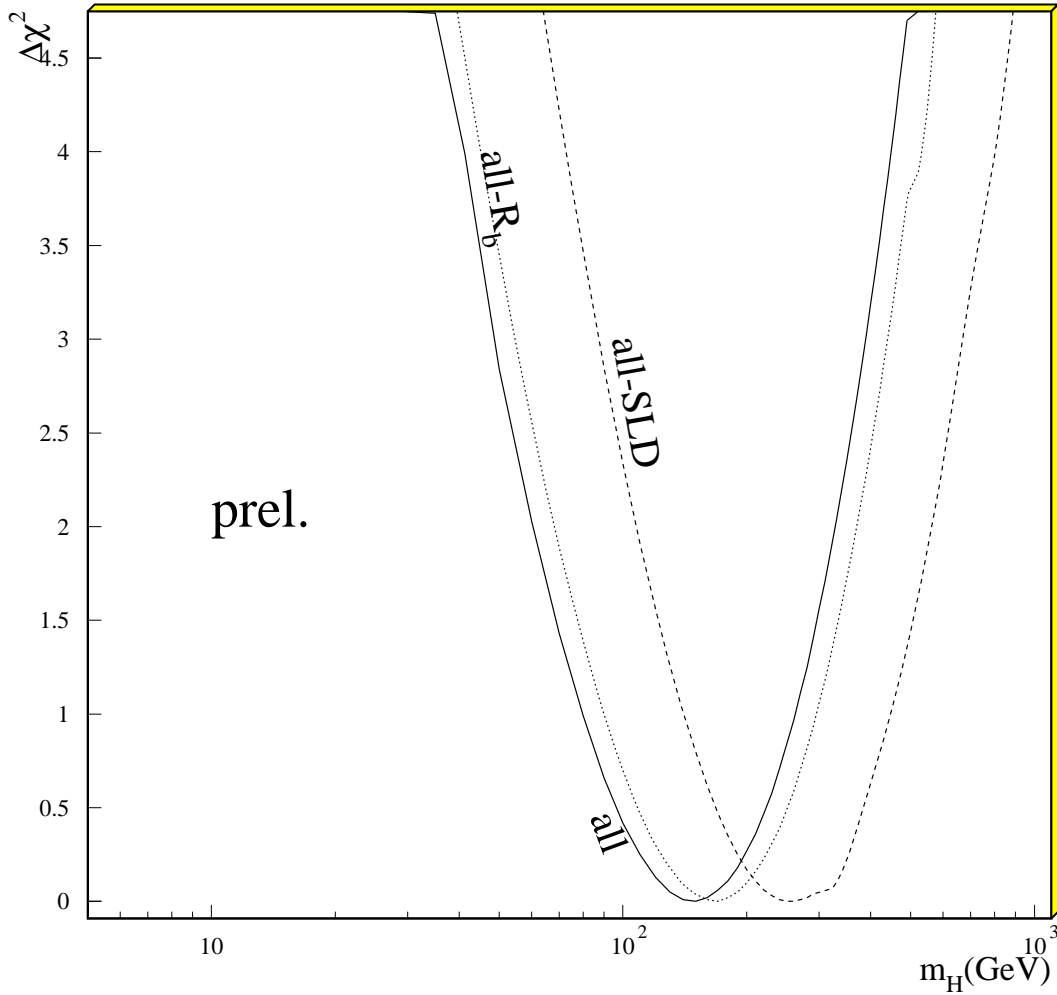


Figure 22: Dependence of the SM  $\Delta\chi^2$  on the Higgs mass for a free top mass, taking all data (continuous line), all data without the SLD measurement of  $\sin^2 \Theta_{eff}^{lept}$  (dashed line) and all data without  $R_b$  (dotted line).

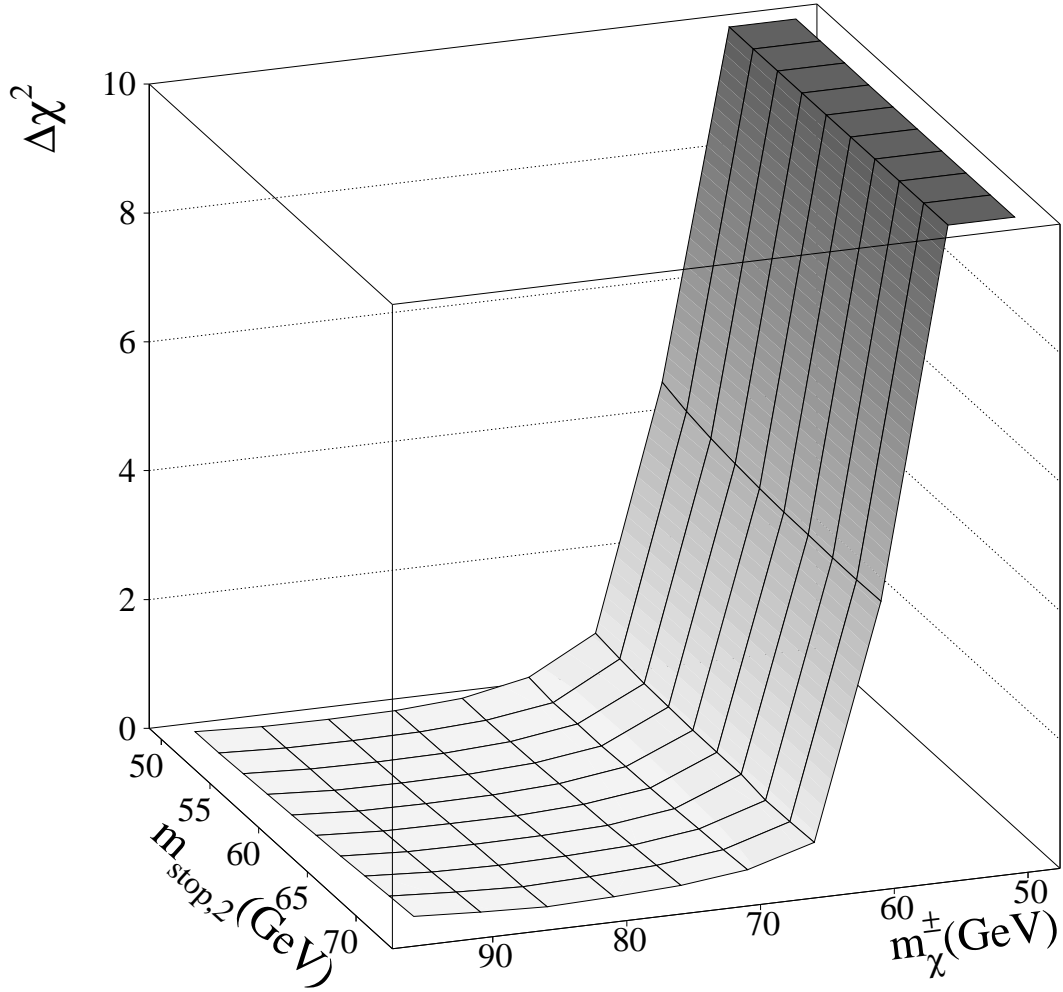


Figure 23: The  $\Delta\chi^2$  in the region of the best fit in the light stop and light chargino plane for  $\tan\beta = 1.6$ . Here the constraint on  $M_2$  was dropped. At each point of the grid an optimization of  $m_t$ ,  $M_2$ ,  $\alpha_s$  and the stop mixing angle  $\phi_{mix}$  was performed with  $\mu > -40$ , including the ratio  $b \rightarrow s\gamma$  and the requirement  $\Gamma_{Z \rightarrow \text{neutralinos}} < 2$  MeV.

Data / MSSM( $\tan\beta = 1.6$ )  
Data / SM (prel.)

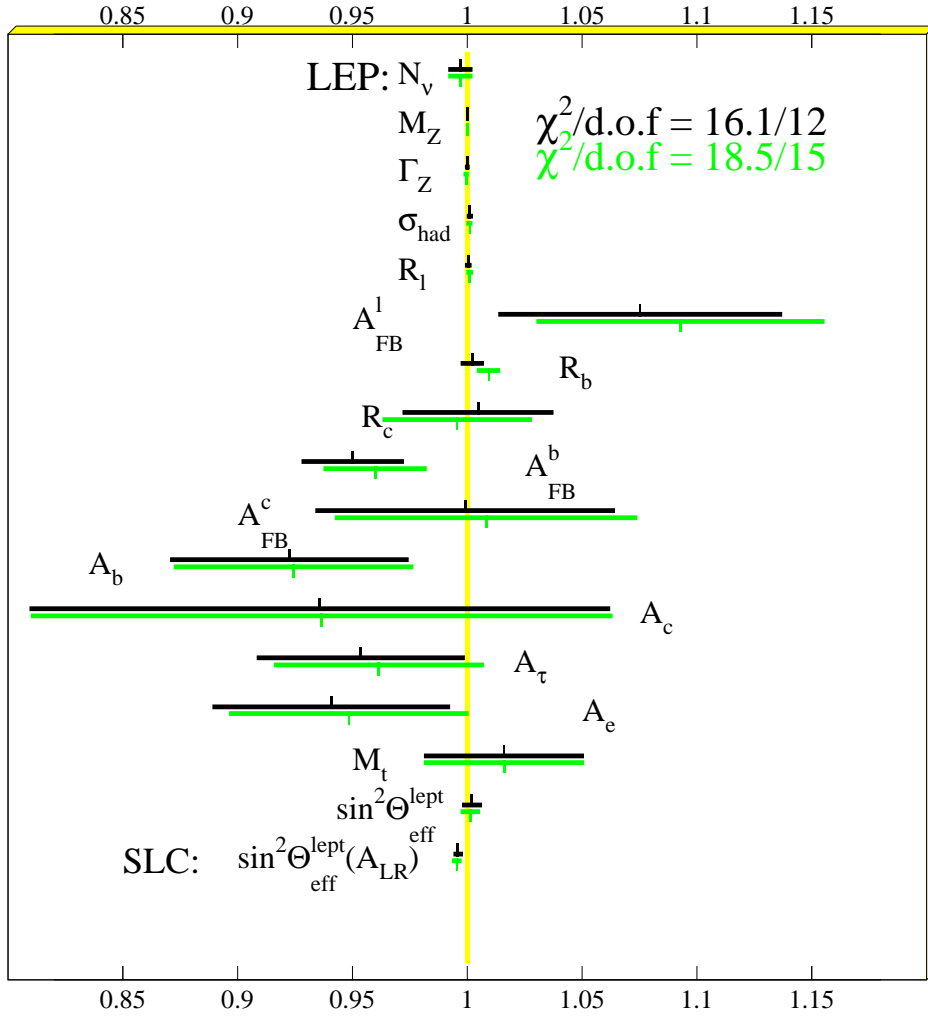


Figure 24: Resulting observables for the fit given in table 3 for  $\tan\beta = 1.6$ .  $\tilde{m}_b$  was fixed to 1000 GeV,  $m_A$  and the gluino mass were fixed to 1500 GeV. Including  $b \rightarrow s\gamma$  in the fit it is still possible to improve the prediction of  $R_b$  with Supersymmetry a bit.

Data / MSSM( $\tan\beta=34$ )  
Data / SM (prel.)

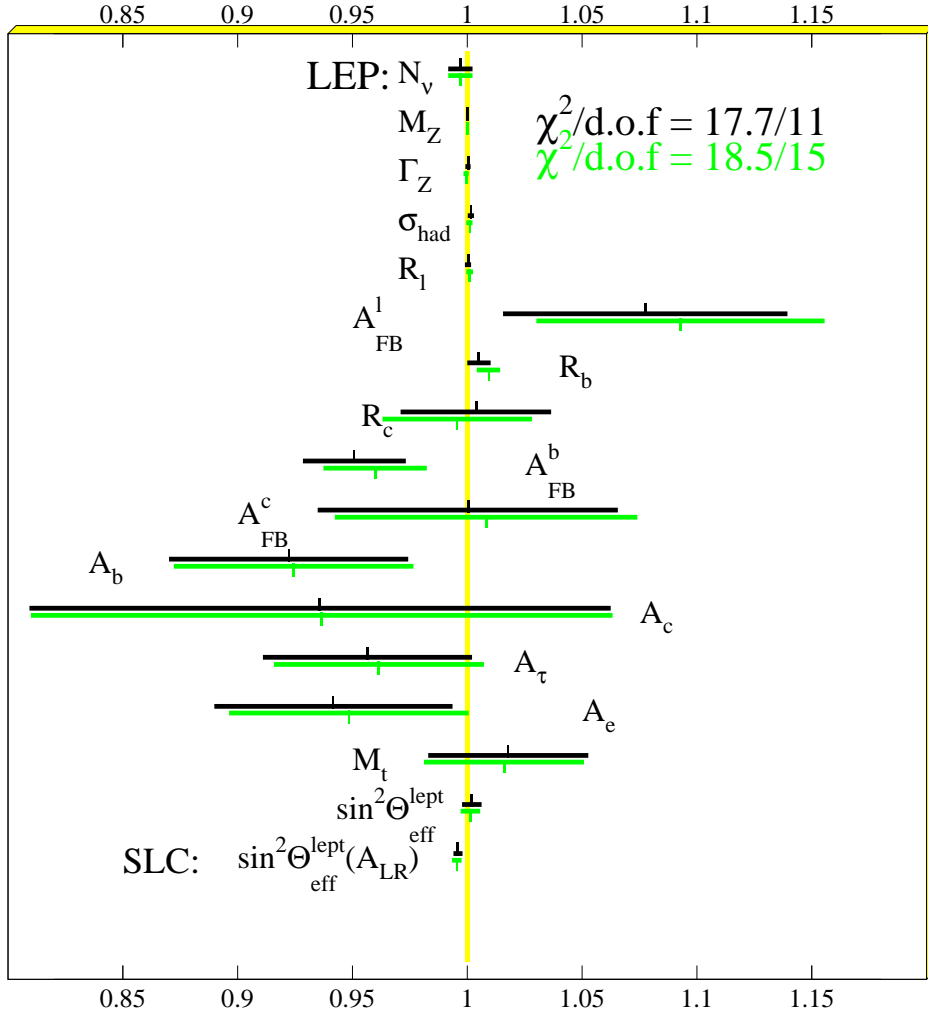


Figure 25: Resulting observables for the fit given in table 3 for  $\tan\beta = 50$ .  $\tilde{m}_b$  was fixed to 1000 GeV,  $M_2$  and the gluino mass were fixed to 1500 GeV. It is possible to improve the prediction of  $R_b$  with Supersymmetry even for high values of  $\tan\beta$ , but the result is not as good as for low values.

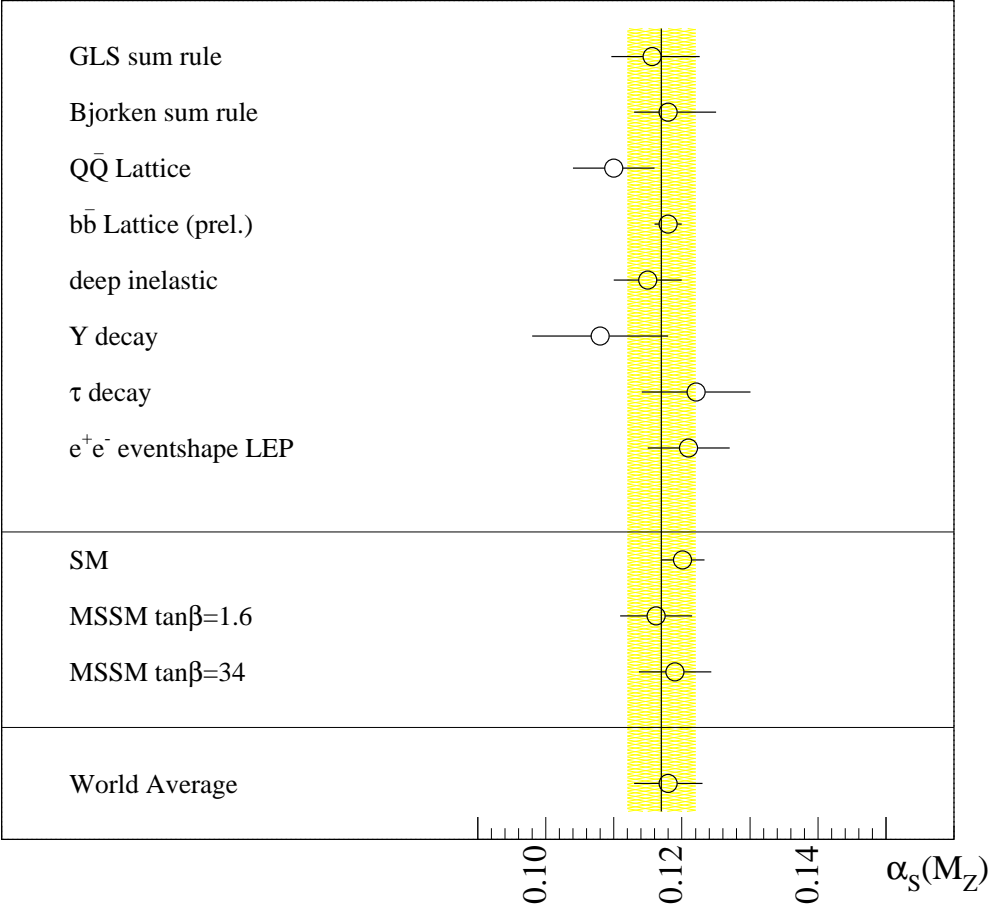


Figure 26: Comparison of different measurements of  $\alpha_s$  with our fit results, labeled SM and MSSM. The data has been taken from [19] and [40].

## References

- [1] *Proceedings of the Workshop Physics at LEP2* , Editors G. Altarelli, T. Sjöstrand, F. Zwirner, Vol.1 and Vol.2, CERN 96-01
- [2] M. Boulware, D. Finnell, *Radiative Corrections to  $BR(Z \rightarrow b\bar{b})$  in the Minimal Supersymmetric Standard Model*, *Phys. Rev.* **D44**(1991) 2054
- [3] P. H. Chankowski, S. Pokorski, *Chargino Mass and  $R_b$  Anomaly* , IFT-96/6, hep-ph 9603310
- [4] J. Ellis, J. L. Lopez, D. V. Nanopoulos, hep-ph/9512288;
- [5] D. Garcia, J. Sola, *The Quantum Correlation  $R_b - R_c$  in the MSSM: More Hints of Supersymmetry?* , hep-ph/9502317, *Phys. Lett.* **B354** (1995) 335,
- [6] G.L. Kane, R.G. Stuart, J.D. Wells, *A Global Fit of LEP/SLC Data with Light Superpartners*, *Phys. Lett.* **B354**(1995) 350, UM-TH-94-16, hep-ph/9505207
- [7] J.D. Wells, C. Kolda, G.L. Kane, *Implications of  $\Gamma(Z \rightarrow b\bar{b})$  for Supersymmetry Searches and Model-Building* , *Phys. Lett.* **B338**(1993) 219, UM-TH-94-23, hep-ph/9408228
- [8] D. Garcia, R. Jimenez, J. Sola, *Supersymmetric Electroweak Renormalization of the Z Width in the MSSM.**Phys. Lett.* **B347** (1995) 309; *Phys. Lett.* **B347** (1995) 321
- [9] D. Garcia, J. Sola, *Matching the low-Energy and the high-Energy Determinations of  $\alpha_s(M(Z))$  in the MSSM*,*Phys. Lett.* **B357**(1995) 349
- [10] A.Blondel, Plenary talk at 28th Int. Conf. on High Energy Physics, Warsaw, July, 1996; LEP Electroweak Working Group, *CERN-preprint* LEPEWWG/96-02, July 1996.
- [11] F. Abe et al., *CDF Collaboration*, Measurements of the W Boson Mass, *Phys. Rev.* **D52** (1995) 4784;  
C. K. Jung, *DØ Collaboration*, W Mass Measurements from DØ and CDF Experiments at the Tevatron, talk given at the 27th ICHEP, Glasgow, Scotland, 20-27 July 1994.
- [12] F. Abe et al., *CDF Collaboration*, *Phys. Rev. Lett.* **74** (1995) 2626, March 1995.  
S. Abachi et al., *DØ Collaboration*, *Phys. Rev. Lett.* **74** (1995) 2632, March 1995.;  
CDF Collaboration, A.Caner, presented at Les Rencontres de Physique de la Vallée d'Aoste, La Thuile, March 1996  
D0 Collaboration, M.Narain, presented at Les Rencontres de Physique de La Vallée d'Aoste, La Thuile, March 1996
- [13] LEP Electroweak Working Group, *CERN-preprint* LEPEWWG/96-01, March 1996.
- [14] CLEO-Collaboration, R. Ammar et al., *Phys. Rev. Lett.* **74**, (1995) 2885
- [15] ALEPH Collaboration, *Search for supersymmetric particles on  $e^+e^-$  collisions at centre-of-mass energies of 130 and 136 GeV*, CERN-PPE/96-10

- [16] OPAL Collaboration, *Topological Search for the Production of Neutralinos and Scalar Particles*, CERN-PPE/96-019;  
*Search for Chargino and Neutralino Production Using the OPAL Detector at  $\sqrt{s} = 130 - 136$  GeV*, CERN-PPE/96-020;  
DELPHI Collaboration, *Search for the Lightest Chargino at  $\sqrt{s} = 130$  and  $136$  GeV*, CERN-PPE/96-75
- [17] D0 Collaboration, *Search for Light Top Squarks in  $p\bar{p}$  Collisions at 1.8 TeV*, *Phys. Rev. Letters* **76**, 2222 (1996), FERMILAB-PUB-95/380-E;  
DELPHI Collaboration, *Search for neutralinos, scalar leptons and scalar quarks in  $e^+e^-$  interactions at  $\sqrt{s} = 130$  GeV and  $136$  GeV*, in preparation
- [18] ALEPH Collaboration, *Mass Limit for the Standard Model Higgs Boson with the full LEP I ALEPH Data Sample*, CERN PPE/96-079
- [19] *Particles and Fields*, *Phys. Rev.* **D50** (1994), 1173-1826, Number 3;  
R.M. Barnett et al., *Phys. Rev.* **D54** (1996) 1.
- [20] D. Bardin et al., *ZFITTER, An Analytical Program for Fermion Pair Production in  $e^+e^-$  Annihilation*, CERN-TH.6443/92
- [21] A. Dabelstein, W. Hollik, W. Mösle, in preparation.
- [22] F. James, *MINUIT Reference Manual*, Version 94.1, Computing and Networks Division CERN Geneva, Switzerland
- [23] A. Sirlin, *Phys. Rev.* **D 22** (1980) 971.  
W. J. Marciano and A. Sirlin, *Phys. Rev.* **D 22** (1980) 2695.
- [24] D. Garcia and J. Solà, *Mod. Phys. Lett.* **A 9** (1994) 211.  
P.H. Chankowski, A. Dabelstein, W. Hollik, W. Mösle, S. Pokorski and J. Rosiek, *Nucl. Phys.* **B 417** (1994) 101.
- [25] For a recent review see: *Precision Calculations for the Z Resonance*, Yellow report CERN 95-03, eds. D. Bardin, W. Hollik and G. Passarino, and references therein.
- [26] L. Avdeev, J. Fleischer, S. Mikhailov and O. V. Tarasov, *Phys. Lett.* **B 336** (1994) 560.  
J. Fleischer, O. V. Tarasov and F. Jegerlehner, *Phys. Lett.* **B 319** (1993) 249;  
R. Barbieri, M. Beccaria, P. Ciafaloni, G. Curci, A. Vicere, *Phys. Lett.* **B288** (1992) 95;  
*ibid.* **B409** (1993) 105;  
K.G. Chetyrkin, J.H. Kuehn, M. Steinhauser, *Phys. Lett.* **B351** (1995) 331;  
J. Fleischer, F. Jegerlehner, P. Raczka, O.V. Tarasov, *Phys. Lett.* **B293** (1992) 437;  
G. Buchalla, A.J. Buras, *Nucl. Phys.* **B398** (1993) 285
- [27] K. G. Chetyrkin, J. H. Kühn and A. Kwiatkowski, *Phys. Lett.* **B282** (1992) 221;  
K. G. Chetyrkin and A. Kwiatkowski, *Phys. Lett.* **B305** (1993) 285;  
K. G. Chetyrkin, A. Kwiatkowski and M. Steinhauser, *Mod. Phys. Lett.* **A 29** (1993) 2785;  
A. Kwiatkowski, M. Steinhauser, *Phys. Lett.* **B344** (1995) 359;  
K. G. Chetyrkin, J. H. Kühn and A. Kwiatkowski, in: *Precision Calculations for the Z Resonance*, CERN 95-03, eds. D. Bardin, W. Hollik, G. Passarino  
S. Peris, A. Santamaria, CERN-TH-95-21 (1995).

- [28] M. Böhm, W. Hollik and H. Spiesberger, *Fortschr. Phys.* **34** (1986) 687.  
W. Hollik, *Fortschr. Phys.* **38** (1990) 165.
- [29] A. Denner, R. Guth, W. Hollik, J.H. Kühn, *Z. Phys.* **C51** (1991) 695
- [30] A. Dabelstein, *Z. Phys.* **C67** (1995) 495; *Nucl. Phys.* **B456** (1995) 25
- [31] H. P. Nilles, *Phys. Rep.* **110** (1984) 1.  
H. E. Haber and G. Kane, *Phys. Rep.* **117** (1985) 75.  
J. F. Gunion and H. E. Haber, *Nucl. Phys.* **B272** (1986) 1; *Nucl. Phys.* **B402** (1993) 567. J. F. Gunion, H. E. Haber, G. Kane and S. Dawson: *The Higgs Hunter's Guide*, Addison-Wesley 1990.
- [32] J. Ellis, G. Ridolfi and F. Zwirner, *Phys. Lett.* **B257** (1991) 83.
- [33] R. Barbieri, G. Gamberini, G. Giudice, G. Ridolfi, *Nucl. Phys.* **B296** (1988) 75-90.
- [34] R. Barbieri and G. Giudice, *Phys. Lett.* **B309** (1993) 86;  
R. Garisto and J.N. Ng, *Phys. Lett.* **B315** (1993) 372;  
S. Bertolini, F. Borzumati, A. Masiero, and G. Ridolfi, *Nucl. Phys.* **B353** (1991) 591 and references therein;  
N. Oshimo, *Nucl. Phys.* **B404** (1993) 20;  
S. Bertolini, F. Vissani, *Z. Phys.* **C67** (1995) 513, 1995
- [35] A. J. Buras et al., *Nucl. Phys.* **B424**(1994) 374
- [36] R. Ehret, *Die Bestimmung der Kopplungskonstanten  $\alpha_s$  am LEP-Speicherring und Tests von großen Vereinigungstheorien*, Ph.D. Thesis, Univ. Karlsruhe, IEKP-KA/95-13
- [37] W. de Boer et al., *Combined Fit of Low Energy Constraints to Minimal Supersymmetry and Discovery Potential at LEP II*, hep-ph/9603350
- [38] S. Eidelman and F. Jegerlehner, *Z. Phys.* **C67** (1995) 585;  
H. Burkhardt and B. Pietrzyk, *Phys. Lett.* **B356**(1995) 398
- [39] W. de Boer et al., *MSSM predictions of the Neutral Higgs Boson Masses And LEP- II Production Cross- Sections*, hep-ph/9603346 and references therein.
- [40] M. Schmelling, Plenary talk at 28th Int. Conf. on High Energy Physics, Warsaw, July, 1996